

# **Re-programing chromatin with a bifunctional LSD1/HDAC inhibitor induces therapeutic differentiation in DIPG**

Jamie N. Anastas<sup>1,2</sup>, Barry M. Zee<sup>1,2</sup>, Jay H. Kalin<sup>3,4</sup>, Mirhee Kim<sup>5</sup>, Robyn Guo<sup>6</sup>, Sanda Alexandrescu<sup>7,8</sup>, Mario Andres Blanco<sup>9</sup>, Stefanie Giera<sup>10</sup>, Shawn M. Gillespie<sup>11</sup>, Jayanta Das<sup>12</sup>, Muzhou Wu<sup>13</sup>, Sarah Nocco<sup>13</sup>, Dennis M. Bonal<sup>14</sup>, Quang-De Nguyen<sup>14</sup>, Mario L. Suva<sup>11,15</sup>, Bradley E. Bernstein<sup>11,15</sup>, Rhoda Alani<sup>13</sup>, Todd R. Golub<sup>15,16,17</sup>, Philip A. Cole<sup>3,4</sup>, and Mariella G. Filbin<sup>8,15\*</sup>, Yang Shi<sup>1,2\*</sup>

<sup>1</sup>Division of Newborn Medicine and Epigenetics Program, Department of Medicine, Boston Children's Hospital, Boston, MA 02115, USA

<sup>2</sup>Department of Cell Biology, Harvard Medical School, Boston, MA 02115, USA

<sup>3</sup>Department of Biological Chemistry and Molecular Pharmacology, Harvard Medical School, Boston, MA 02115, USA

<sup>4</sup>Division of Genetics, Department of Medicine, Brigham and Womens Hospital, Boston, MA 02115, USA

<sup>5</sup>NYU Medical School, New York, NY 10016, USA

<sup>6</sup>Duke University, Durham, NC 27708, USA

<sup>7</sup>Department of Pathology Boston Children's Hospital, Boston, MA 02115, USA

<sup>8</sup>Department of Pediatric Oncology, Dana-Farber Cancer Institute and Children's Hospital Cancer Center, Boston, MA 02215, USA

<sup>9</sup>Department of Biomedical Sciences, School of Veterinary Medicine, University of Pennsylvania, Philadelphia, PA 19104, USA

<sup>10</sup>Sanofi, Cambridge, MA 02139, USA

<sup>11</sup>Department of Pathology and Center for Cancer Research, Massachusetts General Hospital and Harvard Medical School, Boston, MA 02114, USA

<sup>12</sup>Eshelman School of Pharmacy, UNC Chapel Hill, Chapel Hill, NC 27599, USA

<sup>13</sup>Department of Dermatology, Boston University School of Medicine, Boston, MA 02118, USA

<sup>14</sup>Lurie Family Imaging Center, Center for Biomedical Imaging in Oncology, Dana-Farber Cancer Institute, Boston, MA 02215, USA.

<sup>15</sup>Broad Institute of Harvard and MIT, Cambridge, MA 02142, USA

<sup>16</sup>Koch Institute for Integrative Cancer Research, Massachusetts Institute of Technology, 500 Main Street, Cambridge, MA 02142, USA

<sup>17</sup>Howard Hughes Medical Institute, 4000 Jones Bridge Road, Chevy Chase, 20815 MD, USA

\*These authors are co-senior and co-corresponding authors.

## SUMMARY

Histone H3 Lys<sup>27</sup> to methionine mutations (H3K27M) cause epigenetic dysfunction and are frequently observed in Diffuse Intrinsic Pontine Glioma (DIPG), a pediatric brain tumor with no cure. We conducted a CRISPR screen to identify chromatin regulators that might be targeted to treat DIPG in combination with histone deacetylase (HDAC) inhibitors. This screen revealed that genetic ablation of lysine specific demethylase 1 (*LSD1*) sensitizes primary DIPG cells to HDAC inhibitors. Consistently, a bifunctional inhibitor of HDACs and LSD1, Corin, inhibits DIPG growth *in vitro* and in xenografts *in vivo*. Mechanistically, Corin increases global levels of H3K27me3 typically suppressed by the dominant effects of H3K27M mutant histones and simultaneously increases HDAC-targeted H3K27ac and LSD1-targeted H3K4me1 to activate chromatin associated with neuronal genes and at binding sites for REST and other transcription factors. Further studies reveal that Corin treatment results in cell death, cell cycle arrest, and the induction of a neural differentiation phenotype both *in vitro* and *in vivo*. Importantly, Corin-induced transcriptional signatures are overrepresented in normal brain compared to DIPG tumors and correlate with increased survival time in DIPG patient populations. These data suggest a novel strategy for treating DIPG by co-targeting LSD1 and HDACs.

## INTRODUCTION

Pediatric high grade gliomas (pHGGs) are among the most malignant brain tumors of childhood, with no effective treatments despite decades of clinical trials evaluating multiple strategies including various combinations of radiation, chemotherapy, and investigational drugs (Johung and Monje, 2017; Jones et al., 2016; Juratli et al., 2017). Sequencing of pHGGs has recently identified mutations in genes encoding histone proteins (Schwartzentruber et al., 2012; Wu et al., 2012), which are key hubs of epigenetic regulation (Strahl and Allis, 2000). High-grade gliomas of the brainstem termed Diffuse Intrinsic Pontine Gliomas (DIPG), occur in young children and harbor non-synonymous histone mutations resulting in a Lys<sup>27</sup> to methionine (M) substitution in H3.3/H3.1 (H3K27M), in more than 80% of cases (Juratli et al., 2017; Khuong-Quang et al., 2012; Schwartzentruber et al., 2012; Sturm et al., 2012; Wu et al., 2012). Functional studies suggest that H3K27M mutations act as drivers or accelerators of DIPG growth *in vitro* and in animal models, suggesting that epigenetic mis-regulation may promote DIPG tumorigenesis (Cordero et al., 2017; Harutyunyan et al., 2019; Larson et al., 2019; Pathania et al., 2017).

Defective chromatin regulation is characteristic of many cancers, and can regulate tumor phenotypes such as, intra-tumoral heterogeneity, the development of drug resistance, and metastasis (Easwaran et al., 2014; Mack et al., 2016). Given that the H3K27M substitution observed in DIPG is found in the histone tail region that is subject to extensive covalent modification, it has been hypothesized that these mutations might disrupt the pattern of chromatin modifications leading to epigenetic mis-regulation (Fontebasso et al., 2013; Jones and Baker, 2014; Lewis et al., 2013; Schwartzentruber et al., 2012; Wu et al., 2012). In support of this hypothesis, H3K27M mutant tumors and cell lines exhibit reduced H3K27me3 and



H3K27me2 (Bender et al., 2013; Chan et al., 2013; Lewis et al., 2013; Venneti et al., 2013). Moreover, overexpression of H3K27M results in a global reduction of H3K27me3, whereas CRISPR-targeting of the K27M mutation in DIPG cell lines leads to increased H3K27me3 at genomic regions previously associated with K27M mutant histones, suggesting a causal role for K27M in disrupting methylation (Bender et al., 2013; Chan et al., 2013; Harutyunyan et al., 2019; Lewis et al., 2013). Mechanistic studies reveal that the K27M-dependent reduction in H3K27me3 may involve a direct interaction between the mutant histone and the PRC2 methyltransferase complex (Bender et al., 2013; Jiao and Liu, 2015; Justin et al., 2016; Lewis et al., 2013), and that H3K27M mutant histones act in a dominant manner to disrupt EZH2-dependent histone methylation.

In addition to reduced H3K27me3 levels, K27M mutant tumors also exhibit disruptions in the methylation of other histone tail residues including, H3K4me3 and H3K36me2 (Larson et al., 2019; Stafford et al., 2018), as well as potential aberrations in histone acetylation patterns (Nagaraja et al., 2017; Piunti et al., 2017), and a reduction in DNA 5mC-methylation (Bender et al., 2013; Sturm et al., 2012). These data suggest pleiotropic consequences of the H3K27M mutation resulting in the disruption of multiple chromatin regulatory pathways. However, the mechanisms governing each of these potentially H3K27M-dependent deviations in chromatin and DNA modification states and their roles in promoting DIPG tumorigenesis are not fully understood.

We hypothesized that aberrant regulation of chromatin induced by H3K27M mutant histones not only drives DIPG tumor growth, but will also render tumors with H3 mutations vulnerable to epigenetically-targeted therapies alone or in combination with other treatments. In line with this hypothesis, previous studies have shown that small molecule inhibitors of

bromodomain containing proteins such as, BRD4 (Nagaraja et al., 2017; Piunti et al., 2017), EZH2 (Mohammad et al., 2017; Piunti et al., 2017), and histone deacetylases (HDACs) (Grasso et al., 2015) can inhibit DIPG grown *in vitro* and *in vivo*. While these studies highlight the potential promise of epigenetic-therapies for DIPG, the high failure rate of monotherapies in clinical trials suggests that a combinatorial approach might be needed before improved patient outcomes are observed.

In a search for more effective therapies for DIPG, we performed a chromatin-focused CRISPR screen to identify factors that might be co-targeted to enhance H3K27M mutant DIPG growth inhibition by HDAC inhibitors (currently in clinical trials for DIPG: NCT02420613, NCT02274987, NCT03566199, NCT02717455). Our screen discovered that genetic ablation of lysine-specific demethylase 1 (*LSD1*, encoded by *KDM1A*) sensitized DIPG cells to HDAC inhibition. We further show that treatment with Corin, a novel, bifunctional fusion compound targeting both LSD1 and HDACs (Kalin et al. 2018), results in a stronger inhibition of DIPG growth than either HDAC or LSD1 inhibitors alone. We profiled the chromatin landscape and transcriptomes of DIPG cells treated with Corin and observed global changes in histone acetylation and methylation, which correlate with the up-regulation of neuronal differentiation genes and the down-regulation of genes associated with cell cycle progression. Finally, we compared Corin-dependent gene expression profiles with patient RNA-seq data and found that Corin induces a gene signature associated with increased patient survival time. These data suggest that co-targeting LSD1 and HDACs with the dual inhibitor Corin or with similar compounds might be developed as a new strategy for treating DIPG.

## **Significance**

We find that co-inhibiting LSD1 and HDACs with a small molecule, Corin, reduces DIPG growth by re-programing chromatin to inhibit cell cycle and activate a cellular differentiation program. DIPG growth inhibition by Corin is associated with chromatin modification changes that promote the expression of neural differentiation genes but suppress cell cycle genes.

Comparing our RNA-seq data to gene expression profiles from DIPG patient cohorts suggests that Corin-induced gene expression changes correlate with increased patient survival time. Given the complete lack of effective therapies for DIPG, and the dearth of epigenetic inhibitors in general, our data provide evidence for the potential utility of simultaneously inhibiting LSD1 and HDACs with small molecules like Corin to treat DIPG and other cancers driven by epigenetic dysregulation.

## RESULTS

### **A chromatin-focused CRISPR screen identifies LSD1 as a regulator of DIPG sensitivity to HDAC inhibitors.**

To investigate potential roles for chromatin regulators in promoting DIPG growth and survival, we performed a mini screen to determine DIPG cell responses to small molecules from the Structural Genomics Consortium (<http://www.thesgc.org/>) designed to inhibit various epigenetic pathways. We tested the sensitivity of three different patient-derived DIPG cell lines (SU-DIPGXIII, SU-DIPGVI and SU-DIPGIV) that express H3.3/H3.1 H3K27M mutant histones as well as immortalized normal human astrocytes (NHA-hTERT) that express wild type histones as a control. Consistent with previous results, we find that DIPG cells are sensitive to the HDAC inhibitors (HDACi), panobinostat and LAQ824 (Atadja et al., 2004; Dickinson et al., 2009; Grasso et al., 2015), the bromodomain inhibitor, JQ1 (Filippakopoulos et al., 2010; Piunti et al., 2017), and the KDM6A/B demethylase inhibitor, GSK-J4 (Hashizume et al., 2014; Kruidenier et al., 2012) (Figure 1A and Table S1). However, H3.1/H3.3 wildtype NHA-hTERTs appear to be equally sensitive to HDACi and bromodomain inhibitors (Figure 1A and Table S1).

Having confirmed the sensitivity of DIPG cells to HDACi, we next conducted a chromatin-focused CRISPR/Cas9 drop out screen to identify factors that might enhance the response of DIPG cells to the HDACi, panobinostat (also known as LBH-589) (Figure S1A-C). For this screen, we infected Cas9(+) SU-DIPGVI cells with a pooled sgRNA library targeting 1,354 chromatin-associated factors in triplicate. To identify sgRNAs specifically depleted due to HDAC inhibition, we cultured the infected cells for an additional three weeks (~5 doublings) in either control media or media containing a low dose of panobinostat (1.25 nM), before quantifying sgRNA abundance (Figure S1D-E). We identified sgRNAs targeting seventeen

different chromatin regulators to be significantly depleted in the panobinostat-treated samples at a cutoff hit rate of 20% (p-value <0.01) (Figure S1E, Table S2).

One of the top hits was lysine-specific demethylase 1, *LSD1* (*KDM1A*), a histone H3K4me1/2-specific demethylase, which plays important roles in modulating gene expression and in regulating cellular differentiation (Amente et al., 2013; Mosammaparast and Shi, 2010) (Figure S1F). To confirm that co-targeting HDACs and LSD1 synergistically reduces DIPG growth, we generated polyclonal *LSD1* knockout DIPG cell lines by transducing Cas9(+) SU-DIPGVI and Cas9(+) HSJD-DIPG007 cells with control and *LSD1*-targeted sgRNAs. Immunofluorescence microscopy confirmed that >60% of the *LSD1* sgRNA-transduced SU-DIPGVI and HSJD-DIPG007 cells lacked LSD1 protein (Figure S1G-J). Consistent with the results from the screen, culturing these polyclonal *LSD1* knockout lines with either panobinostat, or the structurally distinct HDACi, etinostat, resulted in a loss of the LSD1-depleted nuclei in both SU-DIPGVI (Figure S1G-H) and HSJD-DIPG007 cells (Figure S1I-J). These data are consistent with the hypothesis that loss of *LSD1* impairs DIPG cell survival in the presence of HDAC inhibitors such that *LSD1* knockout cells are no longer observed following HDACi treatment.

### **Co-targeting HDACs and LSD1 with small molecules synergistically impairs DIPG growth *in vitro*.**

Given our genetic data discussed above and reported synergistic anti-tumor effects of HDAC and LSD1 inhibitor combinations in other cancers (Fiskus et al., 2014; Kalin et al., 2018; Singh et al., 2011; Vasilatos et al., 2013), we focused our subsequent studies on targeting LSD1 in DIPG cells together with HDAC inhibitors. We treated primary DIPG cells harboring H3.3 K27M mutations

with combinations of HDACi (panobinostat and etinostat), an LSD1i (compound 7), or a bifunctional fusion compound called Corin (etinostat+compound 7), which inhibits both HDACs 1-3 and LSD1 (Figure S2A) (Kalin et al., 2018). Cell viability assays indicate that treatment with the LSD1i alone had little effect on cell growth, while treatment with HDACi's dose-dependently reduced the viability of five different DIPG cell lines (SU-DIPGVI, SU-DIPGXIII, BT869, BT245, and HSJD-DIPG007) (Figure 1B-D and Figure S2B-F). Consistent with the results of our genetic screen for HDACi sensitizers, combining HDACi with LSD1i resulted in a further reduction in DIPG viability compared to HDACi treatment alone (Figure 1B-D, and Figure S2B-F). This increased toxicity associated with dual inhibition was evident regardless of whether the LSD1i and HDACi were administered as two separate drugs (Figure S2B-D, and S2F) or as the bifunctional fusion molecule, Corin (Figure 1B-D, Figure S2E-F). Importantly, a BLISS independence test confirmed the combinatorial effect of co-treating DIPG cells with compound 7 and etinostat (Figure S2C-D).

To ask whether DIPG cells are uniquely sensitive to co-targeting LSD1 and HDACs we also determined the sensitivity of H3.3/H3.1 wild type NHA-hTERTs to co-treatment with LSD1i and HDACi and find that, although these cells are sensitive to various HDACi's, little further decrease in viability is observed upon Corin treatment (Figure 1E). This result is in line with a previous study showing no synergistic effect of treating NHA-hTERTs with an LSD1i, tranylcypromine and an HDACi, vorinostat (Singh et al., 2011). DIPG cells also exhibit increased sensitivity to Corin compared to non-transformed BJ fibroblasts (Figure 1F), which is consistent with a recent study showing that melanoma cells are more responsive to Corin than non-transformed melanocytes (Kalin et al 2018). These data suggest that there might be a

therapeutic window for treating DIPG with Corin, or other combinations of LSD1 and HDAC inhibitors.

Further studies suggest that the effects of Corin treatment are likely on-target as a Corin analogue (compound 9) (Figure S2A), which does not inhibit LSD1-dependent demethylation (Kalin et al., 2018), failed to synergize with etinostat to impact either HSJD-DIPG007 or BT245 DIPG cell growth, suggesting that inhibition of LSD1 catalytic activity is required for the growth suppressive effects of Corin (Figure S2E). As a further confirmation, we also treated the *LSD1* sgRNA- and control sgRNA-transduced SU-DIPGVI+Cas9 lines (Figure S1G) with etinostat and Corin. Although the LSD1 sgRNA-transduced cells were more sensitive to etinostat than the control sgRNA-expressing cells, no further loss of cells was observed following treatment with Corin (Figure S2G). These data suggest that the enhanced growth-suppressive effects of Corin compared to etinostat are mediated through LSD1 inhibition rather than through an off-target effect of the dual inhibitor.

We then assessed whether short-term treatment with different combinations of LSD1i and HDACi induce DIPG cell death. To this end, we stained SU-DIPGXIII and SU-DIPGVI cells with Trypan Blue 24-48 hours after treatment with the various inhibitors and observed a moderate increase in dead or dying Trypan Blue positive cells following treatment with etinostat and a strong increase in positively stained cells following treatment with Corin (Figure S2H). Treatment with Corin also induced a significant increase in the percent of terminal deoxynucleotidyl dUTP transferase labelled (TUNEL+) SU-DIPGVI cells, suggesting that co-targeting HDACs and LSD1 with Corin leads to increased apoptosis (Figure S2I-J).

## **Dual inhibition of LSD1 and HDACs alters the global patterns of histone modifications in DIPG.**

Previous studies demonstrate that epigenetic regulators that reduce H3K27M mutant DIPG cell growth can increase or decrease H3K27me3 (Grasso et al., 2015; Hashizume et al., 2014; Piunti et al., 2017), which is otherwise repressed by the dominant negative effects of K27M-mutant histones (Bender et al., 2013; Chan et al., 2013; Lewis et al., 2013). To determine whether the LSD1i and HDACi combination can similarly disrupt histone modification patterns in DIPG, we analyzed histones purified from SU-DIPGXIII nuclei after 7 days of treatment with DMSO, compound 7, etinostat, or Corin by liquid chromatography-mass spectrometry (Figure 1G-J, Figure S3A-B, Table S3). These experiments reveal global increases in many different modified histone peptides including HDAC substrates such as, H3.3K27ac and various acetylated histone H4 peptides; the LSD1 substrate, H3K4me1, and even H3K27me3, itself (Figure 1G-J and Table S3). Consistent with the observed greater potency of Corin (Figure 1B-D, Figure S2E-H), both the number of histone modifications that increased or decreased and the magnitude of these changes were greater in Corin-treated cells compared to cells treated with either etinostat or compound 7 alone (Figure 1G-J, Figure S3A-B, and Table S3). Analysis of histone modifications in a second DIPG cell line (SU-DIPGVI) also reveals global changes in histone acetylation and methylation including increases in H3K27me3, H3K4me1 and acetylated H4 due to Corin treatment (Figure S3B and Table S3), suggesting that these Corin-induced changes in chromatin modifications occur across different cell lines. Western blotting confirms that Corin treatment induces more robust changes in histone modifications compared to treatment with the individual inhibitors (Figure 1K).

We next asked whether Corin-induced histone modification changes correlate with the



decreased cell number and increased cell death observed following drug treatment (Figure 1 and Figure S2). We treated HSJD-DIPG007 cells with increasing doses of Corin for 2 or 6 days and monitored histone modifications by Western blotting. Treatment with 0.25  $\mu$ M Corin elevated H3K4me1, H3K27ac, and H3K27me3 after 6 days (Figure 1L, compare lane 8 to 6), and resulted in a corresponding decrease in viable HSJD-DIPG007 cell number (Figure 1N). Treatment with 0.5  $\mu$ M Corin induced more rapid and robust changes in histone modification levels, which correlated with further reductions in viable cell number and a significant increase in dead/dying cells (Figure 1M). In contrast, a lower dose (0.125  $\mu$ M), or shorter treatment time with Corin resulted in no significant loss of viability (Figure 1M-N), and did not induce robust histone modification changes (Figure 1L, compare lane 1 to lanes 2 and lane 6 to lane 7). These data suggest a dose- and time-dependent correlation between Corin-dependent enhancement of histone modification levels and the associated decreases in DIPG cell viability, which we confirmed in a second DIPG cell line (SU-DIPGXIII\*) (Figure S3C-E).

### **ChIP-seq reveals global alterations in H3K4me1, H3K27me3 and H3K27ac modified chromatin in SU-DIPGXIII cells treated with Corin.**

H3K27ac- and H3K27me3-modified chromatin generally correlate with higher gene activation and with gene silencing, respectively, while the combination of H3K27ac and H3K4me1 generally marks active enhancers (Creyghton et al., 2010; Strahl and Allis, 2000), suggesting that Corin-dependent increases in H3K27me3, H3K27ac, and H3K4me1 might re-model the chromatin landscape to regulate gene expression in DIPG. To identify the genomic locations where Corin-induced histone modification changes take place, we next performed ChIP-seq with antibodies detecting H3K4me1, H3K27ac, and H3K27me3 using chromatin extracts from SU-

DIPGXIII cells treated with DMSO or Corin for 7 days. We also performed ChIP-seq with an H3K27M antibody on chromatin isolated from un-treated SU-DIPGXIII cells. Consistent with our analyses of total histone modification levels, we observe an overall increase in H3K4me1, H3K27ac and H3K27me3 ChIP signals in the Corin-treated cells. Specifically, compared to vehicle treated cells, we identified 3,786 H3K27me3, 15,570 H3K27ac, and 6,115 H3K4me1 peaks induced by Corin, whereas only 509 H3K27me3, 85 H3K27ac, and 2,052 H3K4me1 peaks were consistently decreased (FDR <0.01, 2 fold change). Consistent with previous studies suggesting a positive correlation between H3K27ac and H3K27M peaks (Harutyunyan et al., 2019; Nagaraja et al., 2017; Piunti et al., 2017), the top K27M-enriched sites were enriched in H3K27ac compared to sites with lower K27M levels (Figure 2A-B, upper panels). These K27M-enriched sites are also associated with increased H3K4me1 and both the H3K27ac and H3K4me1 signal were modestly increased upon Corin treatment (Figure 2A-B). Interestingly, we also observe a large number of regions characterized by relatively lower levels of K27M binding where Corin treatment promotes even stronger increases in both H3K4me1 and H3K27ac signal, suggesting the establishment of a more activated chromatin state (Figure 2A-B, middle panels). Finally, we observe regions with very low levels of K27M and higher baseline levels of H3K27me3, which were further increased due to Corin treatment (Figure 2A-B, bottom panels), suggesting that these chromatin regions are likely to become more silenced upon drug treatment. We next analyzed the distribution of the K27M-enriched, Corin-activated, and Corin-silenced regions relative to various coding and non-coding regions of the genome (Ji et al., 2006). Regions acquiring increased H3K4me1 and H3K27ac due to Corin treatment (“Corin-activated” chromatin) are localized to promoters ( $p\text{-value} = 9.03 \times 10^{-113}$ ) and 5'-UTRs ( $p\text{-value} = 9.14 \times 10^{-207}$ ), and are also frequently found in introns and intergenic regions potentially acting as distal or

intronic enhancers (Figure 2C). Regions that gained H3K27me3 (“Corin-silenced” chromatin) are similarly enriched in both promoters ( $p\text{-value} = 2.62 \times 10^{-78}$ ) and intergenic regions (Figure 2C). These results suggest that Corin treatment potentially augments or suppresses both promoters and enhancers by inducing simultaneous increases in H3K4me1 and H3K27ac or by depositing H3K27me3, respectively.

We next searched for potentially enriched transcription factor binding sites in chromatin regions where Corin induced either a more activated or a more silenced chromatin state (Figure 2A-B, middle and bottom panels). Corin-activated chromatin regions are enriched in binding sites for the pro-apoptotic protein, TP53 (Figure 2D), which is consistent with our observation of increased cell death (Figure S2H-J). Chromatin regions activated by Corin are also enriched in motifs bound by factors such as, RE1-element silencing transcription factor (REST), and the Androgen Receptor (AR), two transcription factors known to associate with LSD1 and HDACs (Hakimi et al., 2003; Metzger et al., 2005; Zambelli et al., 2013) (Figure 2D-E). REST, which is also known as neuron-restrictive silencer factor (NRSF), functions to repress neuronal genes in non-neuronal cells and also to regulate gene networks related to both neural and glial subtype differentiation (Ballas et al., 2005a; Chong et al., 1995; Qureshi et al., 2010; Schoenherr and Anderson, 1995). This correlation suggests that LSD1 and HDACs might associate with REST at these sites to create a repressive chromatin environment for gene silencing in un-treated cells, and that Corin treatment blocks the removal of activating chromatin marks by LSD1 and HDACs at these regions. This hypothesis is exemplified by the observation of increased H3K27ac and H3K4me1 near predicted REST-binding sites at the *CELSR1* gene locus (Figure 2F), which encodes a regulator of neural progenitor cell differentiation and brain development (Boucherie et al., 2018; Feng et al., 2012). Corin-induced changes in chromatin at REST binding sites can also

be seen on a more global scale, suggesting that the levels of H3K27ac and H3K4me1 are increased in response to Corin at REST sites on average (Figure S3F). In contrast, regions where Corin induces H3K27me3 are more weakly correlated with transcription factor bound motifs (Figure 2D). Together, these data suggest that simultaneously inhibiting both LSD1 demethylase activity and histone deacetylase activity results in changes in both activating and repressive chromatin modification patterns, which may be responsible for the reduction in DIPG growth induced by Corin treatment.

### **Dual inhibition of LSD1 and HDACs results in synergistic gene expression changes.**

To investigate the impact of Corin-induced chromatin modification changes on gene expression, we performed RNA-seq in SU-DIPGXIII cells treated with DMSO, compound 7, etinostat, or Corin for 7 days. Compared to DMSO treatment, compound 7 induces minimal changes in gene expression (Figure 3A, E-F, Table S4), which is consistent with the lack of robust DIPG phenotypes observed in response to LSD1 inhibition alone (Figure 1 and Figure S2). In contrast, HDAC inhibition with etinostat results in many changes in gene expression with 1,178 up-regulated and 264 down-regulated genes, respectively (Figure 3B, E-F, Table S4). Even stronger changes in SU-DIPGXIII cell transcription are induced by Corin treatment with 2,937 up-regulated and 2,070 down-regulated genes ( $p_{\text{adj}} < 0.01$ , 2-fold change) (Figure 3C, E-F, Table S4). These robust changes in gene expression are reflected in a principle component (PCA) analysis of RNA-seq data, suggesting that the transcriptomes of Corin-treated cells are distinct from all other treatment groups (Figure 3D). These data suggest that co-inhibition of LSD1 and HDACs with Corin can induce unique changes in transcription in SU-DIPGXIII cells not observed with either inhibitor alone, which is consistent with the synergistic effect of co-

targeting LSD1 and HDACs on chromatin modification states (Figures 1, 2 and S3) and on DIPG growth (Figures 1 and S2).

We next compared our ChIP-seq and RNA-seq datasets to investigate potential relationships between the global changes in chromatin modifications induced by Corin treatment and the potentially associated changes in gene expression. We first analyzed whether Corin-induced changes in H3K4me1, H3K27ac, or H3K27me3 at promoters correlate with any changes in gene expression. To this end, we generated metagene plots of H3K27ac (Figure 3G, top panels), H3K4me1 (Figure 3G, middle panels), and H3K27me3 chIP signals (Figure 3G, bottom panels) along the promoters and coding regions of genes that are significantly up- (Figure 3G, left panels) and down-regulated (Figure 3G, right panels) by Corin. At the promoters of the Corin up-regulated genes, we observe increases in H3K4me1 and H3K27ac but a slight decrease in H3K27me3 (Figure 3G, left panels), whereas changes in these histone marks at the promoters of down-regulated genes are minor (Figure 3G, right panels).

Since we also observe either increased H3K27me3 or increased H3K27ac and H3K4me1 at many intergenic and intronic regions (Figure 2C), which could be acting as distal enhancers, we also evaluated the potential activation and silencing of distal enhancer elements in response to Corin treatment. We performed a “super enhancer” analysis, where we stitched adjacent regions containing Corin-induced H3K27ac peaks or H3K27me3 peaks together and then ranked these putative enhancers by overall levels of H3K27ac and H3K27me3 as previously described (Figure 3H-I) (Whyte et al., 2013). We then annotated the top “Corin-activated” and “Corin-silenced” enhancers to their nearest genes within 100 kilobases (McLean et al., 2010). As we predicted, genes found near the Corin-activated super enhancers like *TMEM189*, *CEBPB*, *PTPRS*, and *NPTX2* (also known as *NP2*), were all up-regulated by Corin in our RNA-seq data

(Figure 3H, Table S4). In contrast, Corin induced H3K27me3-silenced chromatin at enhancers associated with genes that were either unaffected by drug treatment (*OR2Z*, *ZNF558*, and *TAC4*), or at genes that were down-regulated by Corin such as, *TLE3* and *BMII* (Figure 3I, Table S4), a putative regulator of glioma brain tumor initiating cells (Jin et al., 2017).

Our observation that increased H3K27ac/H3K4me1 either at the promoters of up-regulated genes or at distal enhancer-like elements found adjacent to the up-regulated genes suggests that the induction of these histone marks might promote gene expression. However, it is not clear whether these chromatin modification changes are a cause or a consequence of transcriptional activation. We treated SU-DIPGXIII cells with a short time course of Corin and find that H3K27ac was weakly increased within 2-4 hours and strongly increased after 8 hours (Figure 3J), whereas two Corin target genes (*NEFL* and *SEMA3C*) were not significantly up-regulated until at least 24 hours after starting drug treatment (Figure 3K-L), suggesting that increased H3K27ac precedes the up-regulation of at a subset of Corin target genes.

### **Dual inhibition of LSD1 and HDACs with Corin induces differentiation in DIPG.**

What are the functional consequences of the altered chromatin and transcriptional profiles of DIPG cells treated with Corin? To address this question, we performed gene ontology (GO) analysis (Ashburner et al., 2000) on the up-regulated genes, and found that Corin induces transcripts associated with brain development and neurogenesis, while treatment with etinostat induces genes associated with the development of other tissues such as the cardiovascular and circulatory systems (Figure 4A). We validated some of these gene expression changes by qRT-PCR and observe that Corin treatment results in the up-regulation of genes expressed in more mature neurons (Figure 4B), and the down-regulation of oligodendrocyte progenitor cell (OPC)

and neuronal progenitor cell (NPC) markers (Figure 4C). Since DIPGs are highly heterogeneous tumors, we validated that Corin treatment up-regulated genes associated with neuronal differentiation in a majority of DIPG cell lines tested (Figure 4D-E), while the progenitor marker, *CSPG4* (also known as *NG2*), was down-regulated in 3 out of 5 cell lines (Figure 4F). These data suggest that Corin treatment induces gene expression changes associated with an aberrant neuronal differentiation phenotype in multiple patient-derived DIPG cell lines. Consistent with the RNA-seq data, immunostaining of Corin-treated cells also detected an increase in the percent of cells expressing NP2 (encoded by *NPTX2*), and the REST/NRSF target *CALB1* (*Calbindin 1*) (Ballas et al., 2005a) (Figure 4G), which mark subsets of neurons (Pfyffer et al., 1987; Usoskin et al., 2014). Furthermore, Corin also enhances the formation of neurite-like cell processes in SU-DIPGXIII cells (Figure 4H) and results in both an increase in cellular adhesion and the induction of a bipolar morphology suggestive of differentiation in SU-DIPGVI cells (Figure 4G). Collectively, these data suggest that Corin treatment results in both transcriptional and morphological changes indicative of a more neuronal phenotype, implying that Corin treatment may overcome a differentiation block in DIPG.

### **Corin reduces the expression of cell-cycle related genes and induces cell cycle arrest.**

We next performed GO analysis on the gene sets that are significantly down-regulated by the various LSD1 and HDAC inhibitors. Corin treatment significantly down-regulates genes associated with various aspects of the cell cycle including DNA replication and mitosis (Figure 5A). We confirmed the down-regulation of two key cell cycle-related genes, *AURKB* and *CCNB1*, in response to Corin treatment in both SU-DIPGXIII and SU-DIPGVI cells by RT-PCR, whereas treatment with LSD1i or HDACi alone did not affect expression (Figure 5B-C). Corin

treatment similarly down-regulated *AURKB* and *CCNB1* expression in at least three additional DIPG cell lines (BT245, BT869, SU-DIPGXIII\*, and HSJD-DIPG007) (Figure 5D).

Consistently, Corin treatment reduces the percentage of BrdU(+) S-phase SU-DIPGXIII and SU-DIPGVI cells (Figure 5E-F), and also reduces the percent of SU-DIPGXIII cells expressing the proliferative marker, Ki67 (Figure 5G-H). Taken together, these analyses suggest that Corin treatment decreases DIPG cell proliferation and promotes differentiation.

### **Histone H3 mutation status is not sufficient to predict sensitivity to Corin.**

Given the role of H3K27M mutations in promoting gliomagenesis (Cordero et al., 2017; Harutyunyan et al., 2019; Larson et al., 2019; Pathania et al., 2017), we next asked whether the presence of H3K27M mutant histones could determine sensitivity to Corin treatment. To address this question, we used control cell lines lacking the H3K27M mutation to determine if forced expression of mutant histones could sensitize them to Corin (Figure S4). Consistent with previous studies (Bender et al., 2013; Chan et al., 2013; Lewis et al., 2013), we find that over-expression of H3K27M mutant histones in both NHA-hTERTs and murine neural stem cells lacking *tp53* (mNSCs *tp53*<sup>-/-</sup>) results in a global reduction in H3K27me3 compared to over-expression of wild-type H3 (Figure S4A, compare lanes 3 to 4 and lanes 6 to 7). In spite of the observed reduction in H3K27me3, ectopically expressed H3K27M was not sufficient to sensitize either mNSCs or NHA-hTERTs to Corin (Figure S4B-C).

### **Corin treatment reduces DIPG xenograft tumor size and alters tumor phenotypes.**

Given the promising cytotoxic and differentiation-inducing effects of Corin-treatment in cultured, patient-derived DIPG cells we next asked whether Corin-treatment can reduce DIPG



tumor growth *in vivo*. We engineered HSJD-DIPG007 cells and SU-DIPGXIIIP\* cells, which were derived from an aggressive variant of SU-DIPGXIII cells (Qin et al., 2017), to express luciferase and Zs-green fluorescent protein and then transplanted these traceable cells into the pons of immunocompromised mice. Once tumors were established as indicated by small animal bioluminescent imaging (BLI) (Figure 6A), mice were treated by convection enhanced delivery (CED) with 0.03 mg of Corin or vehicle/saline control. For both HSJD-DIPG007 and SU-DIPGXIIIP\* xenografts, we observe a reduction in luciferase activity in response to a single dose of Corin, suggesting that Corin treatment can reduce tumor size (Figure 6A-C).

We also examined the overall histology of the xenografted mouse brains post-mortem. We found that HSJD-DIPG007 cells grew in a highly infiltrative manner, and observed a loss of tumor cell nuclei in the Corin-treated animals (Figure S5A). In contrast, SU-DIPGXIIIP\* xenografts grew in areas that appeared more compact, with infiltration at the edge of the tumor and with leptomeningeal spread (Figure S5B). The histologic response to Corin varied, with a reduction in tumor cells by 28% (counted and averaged tumor nuclei in 10 high power fields) at the site of injection at one end of the spectrum, and more than 80% tumor necrosis at the other end (Figure 6D). Finally, we established orthotopic xenografts using the parental cell line of SU-DIPGXIIIP\* cells, SU-DIPGXIII cells, transplanted in the pons and again treated these tumors with Corin by CED. As seen in the other cell lines, quantification of both normal mouse brain cell nuclei and the abnormal tumor cell nuclei of the xenografted SU-DIPGXIII cells revealed that Corin treatment resulted in a reduction in the percent of tumor cells (Figure S5C-D). Taken together, these data suggest that co-targeting LSD1 and HDACs with Corin results in a reduction in the tumor size in three different DIPG xenograft models characterized by varying growth patterns and levels of aggressiveness.

As described earlier, we observed global changes in histone modification levels in response to Corin treatment in cultured DIPG cells (Figures 1, 2, S3, Table S3). Corin treatment similarly increases the staining intensity for H3K27ac and H3K27me3 in DIPG cells grown *in vivo* (Figure 6E, Figure S5E-F) (Carpenter et al., 2006). Although we observed increased H3K27ac and H3K27me3 at the core of the SU-DIPGXIIIP\* tumors, we did not see increases in staining intensity in either adjacent regions of the pons (Figure 6E), or towards the edge of particularly large primary tumors (Figure S5G), suggesting only partial tissue penetrance, or activity of Corin in the xenograft tissue. As expected, we also observed the induction of Corin target genes associated with neuronal differentiation, such as NP2 and SYNI/II/III, in the Corin-treated SU-DIPGXIIIP\* xenografts by immunofluorescence staining (Figure 6F), suggesting that a subset of the transcriptional changes observed in cultured cells also occur in tumors. Finally, we stained tumor sections with antibodies to detect the proliferative marker, Ki67, which was reduced in Corin-treated xenografts (Figure 6G), and the apoptotic marker, cleaved Caspase3 (c-Caspase3), which was increased at the core of SU-DIPGXIIIP\* xenografts (Figure 6G). These data suggest that Corin treatment induces global changes in chromatin in xenografts, which are associated with the induction of a differentiation and apoptotic response, at the expense of cell proliferation, which is consistent with the phenotypic changes observed in primary cultured cells (Figures S2, 4, and 5).

### **Corin up-regulates genes associated with increased survival time in DIPG patient cohorts.**

We next sought to determine if the LSD1i/HDACi-dependent gene expression changes observed *in vitro* (Figures 3-5) might correlate with the gene expression profiles of primary patient tumors sub-divided by different characteristics. First, we grouped primary DIPG tumor RNA-seq data

(St. Jude, [EGAD00001000793](#)) into “high” and “low” *LSD1* mRNA expression subgroups (Figure 7A) and then identified differentially expressed genes (Table S5). Consistent with the observations that combining both LSD1 and HDAC inhibitor treatment results in cell cycle arrest *in vitro* (Figure 5), and a reduction in Ki67(+) nuclei in SU-DIPGXIIIIP\* xenografts (Figure 6G), we find that tumors with “high” *LSD1* expression also expressed higher levels of transcripts associated with cell cycle progression and mitosis (Figure 7B). In contrast, *LSD1* “low” tumors over-expressed transcripts associated with cell-cell signaling and metabolism (Table S5). Second, we curated data from the literature to identify genes that are over- or under-expressed in DIPG patient samples compared to normal brain (Pathania et al., 2017; Paugh et al., 2011; Saratsis et al., 2014) (Gene Expression Omnibus data sets: GSE95277 and GSE26576). After compiling these gene signatures, we performed a pre-ranked gene set enrichment analysis (GSEAs) (Subramanian et al., 2005), which reveals that Corin inhibits or increases the expression of genes that tend to be over-expressed or under-expressed in DIPG tumors, respectively (Figure 7C). These data suggest that Corin promotes a transcriptional program that is overrepresented in normal brain compared to DIPG tumors, which further supports our hypothesis that Corin induces a differentiation response to make DIPG cells behave more like normal brain cells.

Finally, we examined whether the Corin-dependent gene signature from our RNA-seq experiments correlates with any clinical outcomes by analyzing retrospective gene expression datasets according to patient survival. To this end, we first divided the tumor samples from the St. Jude cohort into “decreased survival” and “increased survival” groups based on the median survival time (Figure 7D). We find that 155 genes are down-regulated and 53 genes are up-regulated in the decreased versus increased survival groups ( $p_{\text{adj}} < 0.05$ , at least 2-fold change)

(Table S5). GSEA analysis reveals that Corin treatment results in the up-regulation of genes that are more highly expressed in the increased survival group (Figure 7E-F). Together, these data suggest that the Corin-induced gene signature we observe *in vitro* correlates with gene expression profiles associated with better patient outcomes in DIPG patient cohorts.

## DISCUSSION

Current treatment strategies have failed children diagnosed with DIPG, as less than 10% of patients survive more than two years post-diagnosis (Jansen et al., 2012). We and others have hypothesized that epigenetic dysfunction in DIPG cells driven by H3.3/H3.1 K27M mutations would make these tumors sensitive to small molecules targeting chromatin regulators (Grasso et al., 2015; Hashizume et al., 2014; Jones and Baker, 2014; Piunti et al., 2017). Our studies reveal that co-inhibiting HDACs and LSD1 with the small molecule, Corin, decreases DIPG growth by inducing differentiation and suppressing cell cycle genes, suggesting that combinatorial targeting of multiple chromatin regulators might be used to treat DIPG.

Previous work suggests that inhibitors of chromatin modifying enzymes such as HDACs and EZH2 can inhibit DIPG growth, yet the efficacy, durability and specificity of these treatments varies across studies (Grasso et al., 2015; Hennika et al., 2017; Mohammad et al., 2017; Wiese et al., 2016). Multidrug treatment regimens are an emerging strategy for the treatment of many cancers, yet optimizing dosing regimens for multiple drugs with varying pharmacokinetics and pharmacodynamics can prove challenging. One possible strategy for overcoming these difficulties is to create molecules capable of inhibiting multiple targets simultaneously. Indeed, recent studies have pointed to the therapeutic potential of bifunctional fusion compounds designed to inhibit multiple targets such as HDAC inhibitors fused with either PI3K (Qian et al., 2012), or cMET inhibitors (Lu et al., 2017), and compounds co-targeting PI3K and MEK (Van Dort et al., 2015). Our study adds to this growing list of examples where bifunctional compounds provide potentially superior efficacies at reducing cancer growth as opposed to single agents.

Clinical trials employing convection enhanced delivery (CED) to deliver small molecules like irinotecan and panobinostat, or radioactive glioma-targeted antibodies (124I-8H9) are currently underway (NCT01502917, NCT03086616, NCT02717455), raising the possibility that CED-based delivery of additional inhibitors might be developed as a therapeutic strategy for DIPG. Our results suggest that Corin delivered via CED can reduce tumor volume in multiple different DIPG xenograft models, providing a proof of principle that combinations of LSD1 and HDAC inhibitors might be used to treat DIPG. However, these models have technical limitations and improvements in the tissue penetrance of Corin and other related molecules are needed to develop combined LSD1/HDAC inhibition as a potential therapy. For example, optimized formulations of Corin, or the synthesis of brain-penetrant pro-drugs may enable efficient uptake of Corin across the blood brain barrier (BBB) allowing for systemic delivery in the future. Alternatively, the FDA-approved drugs, Parnate and Nardil, which act as non-selective LSD1 and monoamine oxidase inhibitors (Culhane et al., 2010; Jambhekar et al., 2017; Prusevich et al., 2014) are known to cross the BBB, and might be combined with HDACi in a drug repurposing strategy. Lastly, new generations of LSD1i, such as T-448 (Matsuda et al., 2019), which also crosses the BBB but has minimal hematological toxicity, might also be used systemically to treat DIPG.

It should be noted, however, that DIPG is not the only cancer type that responds to the synergistic effect of combining LSD1 and HDAC inhibition, as melanoma and other types of cancer cells similarly respond to combinations of LSD1- and HDAC-targeting compounds (Fiskus et al., 2014; Kalin et al., 2018; Singh et al., 2011; Vasilatos et al., 2013). This observation suggests that the strategy of targeting LSD1 and HDACs may be generally applicable to multiple cancer types. Consistent with this notion, our preliminary results suggest

that the K27M mutation is dispensable for Corin response and that both H3.3/H3.1 wild type and G34R/V mutant pHGGs are also sensitive to Corin *in vitro* (unpublished). Nonetheless, our finding of a superior response of DIPG cells to Corin has important implications for considering this combination strategy for DIPG treatment in the future.

Our extensive profiling of chromatin modifications by mass spectrometry and ChIP-sequencing reveals that Corin-treatment induces global changes in histone modifications not observed with either LSD1 or HDAC inhibitors alone. DIPG growth inhibition due to Corin treatment coincides with striking increases in H3K27me3, H3K27ac and H3K4me1 marks as well as many other covalent modifications such as, H2A.Zac, and H4K20me3 whose functional consequences in DIPG are yet to be determined. By ChIP-seq, we observe thousands of genomic regions where Corin increases both H3K27ac and H3K4me1 levels, which are associated with the activation of gene expression driven by both enhancers and promoters. These data are consistent with previous studies characterizing roles for LSD1 in enhancer regulation in hESCs (Whyte et al., 2012) and leukemic cells (Sugino et al., 2017), and suggest that co-inhibition of both H3K27ac deacetylation by HDACs and H3K4me1 demethylation by LSD1 with Corin can synergistically alter chromatin to change the pattern of promoter and enhancer regulation in DIPG.

Paradoxically, inhibitors decreasing either H3K27ac (i.e., BRD4i) or residual H3K27me3 (i.e., EZH2i) correlate with reduced DIPG growth in some contexts (Mohammad et al., 2017; Nagaraja et al., 2017; Piunti et al., 2017). Moreover, H3K27M mutant histones have been associated with localized increases in H3K27ac levels in a previous study (Piunti et al., 2017). These results suggesting that *decreased* H3K27ac and H3K27me3 might lead to slowed DIPG growth appear initially at odds with our observation that robust *increases* in H3K27ac and

H3K27me3 due to Corin treatment similarly correspond with reduced DIPG growth. One possible explanation for this discrepancy is that Corin might induce H3K27ac- and H3K27me3-modified chromatin at unique regions of the genome. Indeed, Corin induces strong increases in H3K4me1 and H3K27ac at many regions lowly bound by H3K27M mutant histones, but induces only minor increase in H3K27ac and H3K4me1 at regions with high levels of H3K27M binding. Interestingly, the Corin-activated chromatin regions tend to be associated with genes involved in cellular differentiation and neurogenesis. This correlation is in contrast to the regions exhibiting potentially reduced H3K27ac and H3K27me3 due to panobinostat and EZH2i treatment in previous studies, which were associated with genes involved in stem cell maintenance and proliferation (Mohammad et al., 2017; Nagaraja et al., 2017). These findings suggest that targeting different classes of chromatin modifying complexes in DIPG may lead to distinct changes in chromatin modification patterns and raises the possibility that several unique strategies of targeting the epigenome might be developed to treat DIPG.

Our further analyses reveal that Corin treatment results in increased H3K4me1 and H3K27ac at genomic regions enriched in binding sites for transcription factors like REST, which plays an important role in silencing neuronal genes in non-neuronal cells (Chong et al., 1995; Laurent et al., 2015; Lee et al., 2005; Schoenherr et al., 1996; Sun et al., 2010). We hypothesize that dual targeting of both histone acetylation and methylation with Corin may allow for more comprehensive and sustained inhibition of transcriptional silencing complexes associated with REST and other transcription factors than either HDAC or LSD1 inhibitors alone. In support of this model, we find that Corin treatment induces many unique transcriptional changes not observed due to treatment with either LSD1 or HDAC inhibitors alone, including the up-regulation of genes involved in neurogenesis and the down-regulation of genes involved in cell



cycle progression. Consistently, recent work shows that REST is overexpressed in a subset of DIPGs and that loss of REST suppresses the growth of DIPG xenografts (Shaik et al., 2018). Together, these studies suggest that co-targeting LSD1 and HDACs might be applied to relieve REST-mediated gene repression and induce therapeutic differentiation in DIPG, a treatment strategy that has shown promise in neuroblastoma, leukemia and lung cancer (Matthay et al., 2009; Mohammad et al., 2015; Schenk et al., 2012; Westerlund et al., 2017).

Previous studies suggest multifaceted roles for REST in regulating diverse developmental processes including the maintenance of both neural and embryonic stem cell pools, the fine-tuning of gene expression during neuronal and glial differentiation, and the preservation of genome integrity (Abrajano et al., 2010; Gao et al., 2011; Johnson et al., 2008; Nechiporuk et al., 2016). In stem cells, REST often acts to repress target genes via the recruitment of co-repressor complexes (Ballas and Mandel, 2005; Lunyak and Rosenfeld, 2005). In contrast, stimulating cellular differentiation can either expel REST from chromatin, or alter REST protein complex composition by increasing the binding of enzymes like p300/CBP and TET3 (Ballas et al., 2005b; Gao et al., 2011; Kuwabara et al., 2004; Perera et al., 2015), which promote gene transcription by increasing histone acetylation and DNA 5-hydroxymethylcytosine (5hmC), respectively. The exact consequences of dual LSD1/HDAC1 inhibition on REST DNA binding dynamics and on REST-associated protein complexes remain to be determined. Moreover, given that only a subset of the sites where Corin induces simultaneous H3K27ac and H3K4me1 or H3K27me3 enrichment harbor REST binding elements, future research may also shed light on if and how LSD1 and HDACs might regulate transcription factor networks in DIPG more broadly.

Finally, our analyses of clinical datasets profiling the transcriptomes of DIPG patient samples reveal that Corin induces a gene signature more closely correlated with gene expression

patterns observed in normal brain tissue compared to DIPG samples. Intriguingly, these Corin-dependent gene expression patterns also correspond with increased patient survival time in a DIPG patient cohort. Further studies will be necessary to confirm whether alterations in the expression of Corin-target genes in patient samples reflect a true change in the transcriptional regulation of the DIPG tumor cells, or simply a change in tumor composition. Regardless, our finding that Corin treatment can induce robust histone modification and gene expression changes in DIPG cells grown *in vitro* and *in vivo* provides a proof of principle that it may be possible to co-target LSD1 and HDACs to reduce the aggressive growth of DIPG cells. Ultimately, this study demonstrates that simultaneously targeting two chromatin-modifying enzymes results in synergistic changes in chromatin state resulting in striking phenotypes not observed when only one class of enzyme is inhibited, and suggests that combinatorial targeting of chromatin modifiers could be developed as a more general strategy for the treatment of cancers.

## STAR★METHODS

### CONTACT FOR REAGENT AND RESOURCE SHARING

Further information and requests for resources and reagents should be directed to and will be fulfilled by the Lead Contacts, Yang Shi ([yang\\_shi@hms.harvard.edu](mailto:yang_shi@hms.harvard.edu)) and Mariella Filbin ([mfilbin@broadinstitute.org](mailto:mfilbin@broadinstitute.org)).

### EXPERIMENTAL MODEL AND SUBJECT DETAILS

#### *Cell culture*

Primary DIPG cells (SU-DIPGXIII, SU-DIPGVI, SU-DIPGIV, SU-DIPGXIIIP\*, HSJD-DIPG007, BT869, BT245), and mouse neural stem cells (mNSCs *tp53*<sup>-/-</sup>) were grown as neurospheres in glioma stem cell media consisting of a 50:50 mixture of DMEM F12 and Neurobasal A medium containing 20 µg/mL hEGF, 20 µg/mL hFGF-154, 10 µg/mL hPDGFAA, 10 µg/mL hPDGFBB, B27 without vitamin A, and 0.02% heparin sulfate, that was supplemented with 1 mM sodium pyruvate, 10 mM HEPES buffer, 1× GlutaMAX, and 1× Antibiotic-Antimycotic. Cells were fed every three to four days with fresh media and drugs where indicated and passaged approximately once per week using TrypLE Express Enzyme to dissociate spheroids to obtain a single cell suspension. NHA-hTERT, BJ fibroblasts and HEK293T cells were maintained in high glucose DMEM containing 10% FBS and 1% penicillin-streptomycin as adherent culture and passaged approximately once every 3 days.

#### *Immunocompromised mice*

Five week old female NSG mice (NOD.Cg-Prkdc<sup>scid</sup> Il2rg<sup>tm1Wjl</sup>/SzJ, The Jackson Laboratory, Bar

Harbor, ME) were used in these studies. All animal studies were performed according to Dana-Farber Cancer Institute Institutional Animal Care and Use Committee (IACUC)-approved protocols.

## **METHOD DETAILS**

### ***Viral production and generation of Cas9-expressing stable cell lines***

To generate lentiviral particles, HEK293T cells were grown to 80% confluence in 10 cm plates and transfected with 8 µg of pCMV-dR8.2-dvpr, 1 µg of pCMV-VSVG-QM2 and 8 µg of transfer plasmid using 25,000 MW polyethylenimine (PEI). The following morning, fresh media was added and viral supernatants were collected at 48 and 72 hours post-transfection and filtered through a 0.45 µm filter. Lentiviral particles from HEK293T supernatants were precipitated overnight at 4°C with 8,000 MW polyethylene glycol (PEG) added to a concentration of 10% w/v followed by centrifugation at 271 RCF for 20 minutes and re-suspension in appropriate media.

To generate stable Cas9(+) DIPG cell lines, SU-DIPGVI, SU-DIPGXIIIP\*, and HSJD-DIPG007 cells were spin infected by first dissociating spheroids with TrypLE™ Express Enzyme, and then centrifuging  $\sim 2 \times 10^6$  cells in each of 12xwells of a 12-well plate in the presence of lentivirus for 90 minutes at 271 RCF. After centrifuging, infected cells were re-suspended and re-plated in T75 suspension culture flasks the presence of lentivirus overnight. The following morning, cells were switched to fresh growth medium, and 48 hours post-infection they were selected with 2-4 µg/mL blasticidin for 7 days to generate stable cell lines. To determine the Cas9 activity, SU-DIPGVI+Cas9 or parental SU-DIPGVI cells were infected with pXPR\_011, which contains both a GFP reporter and a sgRNA targeting GFP. The levels of

GFP in these cell lines was determined by flow cytometry on a FACSDiva (BD Biosciences) followed by analysis using FloJo (<https://www.flowjo.com/>) 1-3 weeks after infection.

To generate polyclonal LSD1 knockout cells, SU-DIPGVI+Cas9 and HSJD-DIPG007+Cas9 cells were spin infected as described above with pLenti\_SpsmB1\_sgRNA\_Hygro containing an LSD1 or control sgRNA targeting sequence and then selected with 300 µg/mL hygromycin for 7 days. HSJD-DIPG007 and SU-DIPGXIII\* cell lines were similarly spin infected with pHIV-Luc-ZsGreen and then sorted based on the ZsGreen signal using a FACSDiva cytometer (BD Biosciences) to generate luciferase-expressing cell lines to be used in xenograft experiments. Finally, NHA-hTERT and mNSCs *tp53*<sup>-/-</sup> expressing various flag-tagged histones were generated by infecting these cells with lentiviruses with wild type H3.3 and K27M mutant H3.3 cloned into a pCDH backbone (pCDH-flag-H3.3), which were kind gifts from Dr. Laura Banaszynski (University of Texas Southwestern). Infected mNSCs *tp53*<sup>-/-</sup> and NHA-hTERTs were then selected by treatment with 600 µg/mL or 1000 µg/mL of G-418 (Research Products International, 108321-42-2), respectively.

### ***Cell viability assays and compound screening.***

For cell viability assays, cells were plated in 96-well plates at densities of 15,000 cells per well (SU-DIPGXIII, SU-DIPGVI, SU-DIPGIV, BT245, BT869, and HSJD-DIPG007 cells), 10,000 cells per well (NHA-hTERT, mNSCs), or 5,000 cells per well (BJ fibroblasts). Corin and other epigenetic inhibitors were re-suspended in DMSO to generate stocks of 10-50 mM and serially diluted in DMSO in order to generate the various dose response curves. Cells were treated with different doses of inhibitors for 6-8 days, and cell viability was determined using the CellTiter-Glo assay according to manufacturer's protocol, which measures ATP as a proxy for cell number

(Promega).

### ***CRISPR Screening***

SU-DIPGVI cells expressing Cas9 were infected with a chromatin-focused sgRNA lentiviral library at a coverage of 1,500 cells per sgRNA in triplicate. Two days after infection, cells were selected for 3 days with 2 µg/mL puromycin (Gold Biotechnology) and then allowed to grow for an additional three days. At this point, reference samples were collected to quantify the initial sgRNA abundance. The remaining infected SU-DIPGVI cells were then passaged into either control media or media containing 1.25 nM panobinostat with triplicate flasks for each condition and grown for an additional three weeks, feeding the cells every 3-4 days with fresh media and panobinostat. After outgrowth for ~5 doublings, surviving cells were harvested, genomic DNA was isolated from all samples and the sgRNA sequences were amplified by PCR before sequencing on a HiSeq2500 sequencer (Illumina). STARS was used to score depleted genes under each condition relative to the reference samples (<https://portals.broadinstitute.org/gpp/public/software/stars>).

### ***Cell death assays***

For Trypan Blue staining, 500,000 SU-DIPGVI or SU-DIPGXIII cells were plated and treated with DMSO, 0.5 µM compound 7, 0.5 µM etinostat, or 0.5 µM Corin for 24, or 48 hours. After treatment, neurospheres were centrifuged and media was removed. 30 µL of TrypLE was used to dissolve the neurospheres, then 270 µL of ice cold 1×PBS and 100 µL of Trypan Blue (Thermo Fisher Scientific, 15250061) were added for a final concentration of 0.1%. Total cells and Trypan Blue positive cells were determined by manual counting on a hemocytometer. For

TUNEL staining, SU-DIPGVI cells were plated on laminin coated coverslips and the treated for two days with 0.5  $\mu$ M of the various compounds before fixing for 20 minutes in 4% para-formaldehyde (PFA), followed by TUNEL staining using the DeadEnd™ Fluorometric TUNEL System (Promega, G3250) following the manufacturer's protocol.

### ***Intracranial xenotransplantation***

To establish DIPG tumors *in vivo* either SU-DIPGXIII cells, HSJD-DIPG007 cells expressing luciferase/Zs-green, or SU-DIPGXIIIP\* cells expressing luciferase/Zs-green were injected stereotactically into the right pons of five week old female NSG mice (NOD.Cg-Prkdc<sup>scid</sup> Il2rg<sup>tm1Wjl</sup>/SzJ, The Jackson Laboratory, Bar Harbor, ME). For the SU-DIPGXIII and HSJD-DIPG007 models, 200,000 cells were injected, while 150,000-300,000 cells were injected for the SU-DIPGXIIIP\* model. Specifically, 150,000 SU-DIPGXIIIP\* cells were injected for comparisons of luciferase signal as a proxy for tumor size after drug treatment and for post-mortem histology, and 300,000 cells were injected before analysis of histone modifications and Corin target genes by immunofluorescence staining.

To prepare for the intracranial injection procedure, animals were injected intraperitoneally with the analgesic buprenorphine 0.05 mg/kg and then anesthetized with 2–3% isoflurane mixed with medical air and placed on a stereotactic frame. The skull of the mouse was then exposed through a small skin incision, and a small burr hole was made using a 25-gauge needle at the selected stereotactic coordinates zeroed on lambda: -1.0 mm X, -0.8 mm Y and 5.0 mm Z for pontine injections. For the injections, DIPG cells were then re-suspended in 4-6  $\mu$ L PBS and loaded on a 33-gauge Hamilton syringe, and injected at rate of 1  $\mu$ L/min with use of an infusion pump. Upon completing an injection, the needle was left in place for another minute, then withdrawn slowly to help reduce cell reflux. After closing the scalp with suture and staple,

mice were returned to their cages placed on a warming pad and visually monitored until full recovery. Mice were then checked daily for signs of distress, including seizures, weight loss, and tremors, and euthanized as they developed neurological symptoms, including head tilt, seizures, sudden weight loss, loss of balance, and/or ataxia. All animal studies were performed according to Dana-Farber Cancer Institute Institutional Animal Care and Use Committee (IACUC)-approved protocols.

### ***Drug Injection by Convection-Enhanced Delivery (CED)***

Mice harboring pontine DIPG xenografts were treated with either Corin or vehicle (DMSO) at the tumor site by CED injection. Before the CED procedure, animals were injected subcutaneously with the analgesic buprenorphine (0.05 mg/kg) and then anesthetized with 2.5–3% isoflurane mixed with medical air. After placing the animals on a stereotactic frame, the skull of the mouse was exposed through a small skin incision, and a small burr hole was made using a 25-gauge needle at lambda: -1.0 mm X, -0.8 mm Y and 5.0 mm Z. The mice were injected with 3  $\mu$ L of Corin dissolved in normal saline with 5% DMSO at a concentration of 0.02 mg/ $\mu$ L by infusion using an autoinjector at a 0.5  $\mu$ L/min rate for a total dose of 0.03 mg of Corin. Vehicle-treated animals were treated with saline/DMSO following the same procedure. Upon infusion, the needle was left in place for another 1-2 minutes, then withdrawn slowly to help reduce reflux. Animals were returned to their cages to recover and resumed normal active behavior within 3–12 hours.



### ***Bioluminescence imaging (BLI)***

Tumor growth was monitored using the IVIS Spectrum In Vivo Imaging System (PerkinElmer), starting at day 7 post-cell injections. Briefly, mice were injected subcutaneously with 75 mg/kg D-luciferin potassium salt (Promega, E1605) in sterile PBS, and anesthetized with 2% isoflurane in medical air. Serial bioluminescence images were acquired using the automated exposure set-up. The peak bioluminescence signal intensity within selected regions of interest (ROI) was quantified using the Living Image Software (PerkinElmer), and expressed as photon flux (p/sec/cm<sup>2</sup>/sr). Representative planar bioluminescence images are displayed with indicated adjusted minimal and maximal thresholds.

### ***Analysis of xenografts and mouse brain tissues by immunofluorescence and using histological stains***

For immunofluorescence staining for histones and differentiation markers, mice xenografted with SU-DIPGXIIIP\* cells were perfused with formalin prior to brain collection. Collected brains were then allowed to equilibrate in 30% sucrose/PBS solution for 24-48 hours. The brains were then embedded in TissueTek (Sakura) and frozen in a bath of ethanol chilled with dry ice. 12 µm sections were obtained on a cryostat. For staining, slides were permeabilized with 0.25% Triton-X-100 in PBS for 20 minutes, blocked with 4% Bovine Serum Albumin (BSA) in PBS plus 0.1% Tween-20 for 45 minutes, and then stained overnight with primary antibodies: H3K27ac (Active Motif, #39135), 1:2000), H3K27me3 (Millipore, 07-449, 1:1000), SYNII/II/II (Biolegend a17080a, 1:1000), or NP2 (1:500, Santa Cruz Biotechnology, sc-166035). The following morning, slides were washed extensively with PBS containing 0.1% Tween-20 (PBST, 4×5 minutes), then incubated for 30 minutes with fluorescent secondary antibodies (Thermo

Fisher Scientific), before washing with PBST again (4×5 minutes), and then incubating the slides with Hoechst diluted in water to 2 µg/mL for 10 minutes to counterstain DNA. For H3K27ac and H3K27me3 quantification, at least 8 images were taken and the level of immunofluorescence signal was determined via CellProfiler (Carpenter et al., 2006) using the Hoechst stain to first segment nuclei and then measuring the signal for H3K27ac and H3K27me3 within the nuclei.

For Hematoxylin and Eosin (HE), Hoechst, cleaved Caspase3, and Ki67 staining mice were also perfused with formalin before their brains were collected and subjected to an additional 24 hour post-fix in formalin. After a brief storage in 70% ethanol, the fixed brains were then embedded in paraffin and sectioned. Prior to staining, brain tumor slides were de-paraffinized with xylenes (3×5 minutes), and then re-hydrated through graded ethanol washes (2×5 minutes 100% ethanol, 2x5 minutes 95% ethanol, 2×5 minutes 80% ethanol, 2×5 minutes water). Antigen retrieval was achieved by boiling in 10 mM trisodium citrate buffer (pH 6.0) for twenty minutes. After blocking in phosphate buffered saline (PBS) with 10% normal goat serum and 1% BSA slides were stained with Hoechst diluted in water to 2 µg/mL for 10 minutes to counterstain DNA before mounting. HE staining was carried out at the Harvard Rodent Histopathology Core using standard protocols and cleaved Caspase3 (antibody #GB11009) and Ki67 (antibody #GB13030-2) staining was performed by ServiceBio (Boston, MA).

To score the percent of SU-DIPGXIII tumor nuclei by the Hoechst stain, at least ten different 20× fields were taken randomly from sections of the hindbrains of xenografted mice. Tumor and non-tumor nuclei were manually scored based on their irregular morphology and lack of defined heterochromatin organization characteristic of normal mouse brain cells. The identity of transplanted cell nuclei was further confirmed by staining with an antibody to detect a human specific nucleolar antigen (Abcam, ab190710 1, data not shown). All slides were blinded before

imaging and scoring to prevent bias. At least 5,000 nuclei were scored per mouse to calculate the average percent SU-DIPGXIII nuclei.

### ***Analysis of histone modifications by mass spectrometry and Western blotting***

To analyze histone modification patterns SU-DIPGVI, or SU-DIPGXIII cells were treated for 7 days with either DMSO, compound 7, etinostat, or Corin at a concentration of 0.5  $\mu$ M. For Western blots, cells were counted, and collected in Laemmli buffer. Alternatively, SU-DIPGXIIIP\* and HSJD-DIPG007 cells were treated with increasing doses of Corin for 2 or 6 days with DMSO, 0.125  $\mu$ M, 0.25, 0.5, or 1.0  $\mu$ M Corin before counting and lysing. After collection, these protein samples were resolved in 15% SDS-PAGE gels. After transferring to nitrocellulose, and blocking with 4% milk dissolved in PBS with 0.1% Tween-20, Westerns were performed using various histone antibodies (see Key Resource Table).

To analyze histone modifications by mass spectrometry, histones were isolated by acid extraction. Briefly, DIPG neurospheres were first dissociated to obtain single cells which were pelleted by centrifugation. Cell pellets were re-suspended in swelling buffer (25 mM Tris-HCl (pH 8.0), 1.5 mM  $MgCl_2$ , 10 mM KCl, 0.2% NP40) containing protease and phosphatase inhibitors and 10 mM sodium butyrate. Nuclei were then isolated by centrifugation at 464 RCF. After washing the collected nuclei once with swelling buffer, they were re-suspended in 0.2N HCl also containing butyrate, and protease and phosphatase inhibitors and extracted overnight at 4°C on a rotator. The following morning, samples were cleared by centrifugation at 21,130 RCF for 30 minutes and supernatants containing extracted histones were removed to fresh microfuge tubes. Trichloroacetic acid was added to these supernatants containing the acid-extracted proteins to a concentration of 30% w/v and proteins were precipitated on ice for one hour before

centrifugation at 21,130 RCF for 30 minutes. Protein pellets were washed with 100% ice cold acetone and then allowed to dry before re-suspension in 50 mM ammonium bicarbonate (pH 8.0). After determining the quality of the samples on an SDS-PAGE gel stained with Coomassie blue, histones were analyzed by mass spectrometry. Histones were derivatized with propionic anhydride (1:3 propionic anhydride:isopropanol prepared prior to use), both before and following trypsin digestion (1:20 trypsin:histone, 50 mM ammonium bicarbonate, 4-6 hours at 37°C); derivatized peptides were then desalted with in-house constructed C18 STAGE tips and analyzed by liquid chromatography-mass spectrometry (LC-MS). Modified peptides were then quantified by chromatographic peak integration as described previously (Zee et al., 2016).

### ***Native ChIP for histones***

For native histone ChIP, SU-DIPGXIII neurospheres amounting to  $5.0 \times 10^6$  cells were treated with 0.5  $\mu$ M Corin or DMSO for 7 days prior to disassociation with TrypL-Express and isolation of nuclei using a hypotonic buffer (25 mM Tris (pH 8.0), 1.5 mM  $MgCl_2$ , 0.2% NP40, 10 mM KCl). Isolated nuclei were washed in buffer A (0.34 M sucrose, 4 mM  $MgCl_2$ , 60 mM KCl, 50 mM HEPES (pH 7.4), and digested with using 0.1  $\mu$ l Micrococcal Nuclease I (New England Biotechnology) per  $1 \times 10^6$  cells to obtain mono- and di-nucleosomes. Micrococcal nuclease reactions were stopped by the addition of EGTA to 10 mM final concentration. Nuclei were then pelleted and chromatin was extracted in 10 mM EDTA with protease and phosphatase inhibitors and 10 mM sodium butyrate added for one hour at 4°C followed by the addition of NaCl to 500 mM and continued incubation at 4°C for an additional hour. After centrifugation at 21,130 RCF at 4°C for 15 minutes, soluble chromatin fractions were removed to fresh tubes and diluted to 100 ng/ $\mu$ l in a buffer containing 20 mM Tris-HCl (pH 8.0), 5 mM EDTA, 500 mM NaCl, and

0.1% Tween-20. Aliquots of diluted chromatin were then incubated overnight at 4°C with 5 µg of the following antibodies: H3K27ac (Active Motif, #39135), H3K4me1 (Abcam, ab8895), or H3K27me3 (Millipore, 07-449). Antibody-chromatin complexes were retrieved using protein G magnetic beads (EMD Millipore), followed by extensive washing and elution in a buffer containing 1% SDS, 50 mM Tris HCl (pH 7.0), and 1 mM EDTA and elution in a buffer containing 50 mM TrisHCl (pH 7.0), 1% SDS, and 1 mM EDTA. Eluted DNA samples were treated with 1 µl of 10 mg/mL RNaseA (Thermo Fisher Scientific) and incubated for 4 hours at 56°C on a thermomixer and then with 5 µl of 20 mg/mL proteinase K (Sigma) and incubated at 55°C overnight. ChIP samples were further purified by phenol-chloroform extraction followed by precipitation by adding ethanol to 67% v/v, sodium acetate to 0.3 M, and 20 µg of glycogen (Roche, 10901393001) and centrifugation at 4°C and 21,130 RCF for 30 minutes. Precipitated ChIPed DNA was re-suspended in water and libraries for sequencing were prepared using the NEBNext library preparation kit (New England Biotechnology) and sequenced on an Illumina HiSeq2500 to a length of 50 base pairs.

### ***Crosslinking chIP for H3K27M***

SU-DIPGXIII cells were crosslinked with 1% formaldehyde added directly to the media for 10 minutes at 37°C before quenching with glycine added to a concentration of 0.11 mM. After pelleting and washing cells twice with PBS, cells were re-suspended in lysis buffer (50 mM Tris-HCl, 1% SDS, 0.25% sodium deoxycholate) with protease inhibitors added and lysed for 10 minutes on ice. After lysis, samples were diluted 1:2.33 with ChIP dilution buffer (50 mM Tris-HCl pH 7.4, 0.01% SDS, 15 mM NaCl, and 1% Triton-X) and then sonicated to 200-3000 base pair fragments. After sonication, samples were diluted another 10 fold in ChIP dilution buffer

and H3K27M immunoprecipitation was done overnight using 5 µg of antibody (Millipore, ABE419) followed by retrieval of immunoprecipitated proteins and DNA with magnetic protein G beads on a rotator at 4°C for 2 hours. Protein G beads were then washed with 1 mL RIPA wash buffer (0.1% SDS, 0.1% sodium deoxycholate 1% Triton X100, 1 mM EDTA, 10 mM Tris-HCl (pH 8.1), 150 mM NaCl), followed by 1 mL of RIPA wash buffer with the NaCl concentration increased to 500 mM, and 1 mL LiCl wash buffer (10 mM Tris-HCl (pH 8.1), 250 mM LiCl, 0.5% TritonX-100, 0.5% sodium deoxycholate), and 1 mL of 10 mM Tris-HCl (pH 8.5). ChIP samples were eluted with a solution of 50 mM Tris-HCl (pH 8.0), 0.1% SDS, 150 mM NaCl and 5 mM dithiotreitol (DTT) at 65° C for 1 hour. Eluates were then subjected to treatment RNase (Roche, 11119915001) at 37°C for 30 minutes followed by treatment with Proteinase K (Sigma, G1508) added to 0.25 mg/mL at 63°C for 3 hours. DNA was then isolated by double sided SPRI bead purification using AMPure XP beads following the manufacturer's protocol (Beckman-Coulter).

Libraries were constructed by first conducting DNA end repair reactions using the End-It DNA End-Repair Kit (Epicenter, ER0720) followed by AMPure XP bead purification and the addition of an adenine base to the 3' end of the end-repaired DNA fragments using Klenow (3'-5' exo-) (New England Biolabs, M0212L). DNA ligase (New England Biolabs, M2200S) was then used to ligate adapter sequences to the libraries, which were then PCR amplified in order to add index sequences using PFU ULTRA II Hotstart 2X PCR master mix (Agilent, 600850). After a final round of size selecting using AMPure XP purification to remove un-incorporated primers and small DNA fragments libraries were then quantified and subjected to high-throughput paired end sequencing to a length of 40 base pairs.

### ***RNA-seq and RT-PCR***

For RNA-seq analysis of gene expression,  $1 \times 10^6$  SU-DIPGXIII cells were treated for 7 days in 0.5  $\mu$ M DMSO, compound 7, etinostat, or Corin, followed by RNA purification and analysis. For RT-PCR analysis of gene expression SU-DIPGXIII, SU-DIPGVI, SU-DIPGXIIIP\*, BT86, BT245, or HSJD-DIPG007 cells were treated for 6-8 days with 0.25-0.5  $\mu$ M of compound 7, etinostat, or Corin. For RT-PCR experiments, RNA extraction and purification was performed using 1 mL of TRIzol® following the manufacturer's protocol (Thermo Fisher Scientific). cDNAs were generated using the PrimeScript™ Reverse Transcriptase Kit (Clontech, RR037B) using both oligoDT and random hexamers in the reaction mixes. RT-PCR standards were generated by PCR-amplification of cDNA using Platinum® PCR SuperMix (Thermo Fisher Scientific, 11306016), and purified by gel extraction using a QIAquick Gel Extraction Kit (Qiagen, 28706) before quantification and serial dilution to generate standard curves. RT-PCR reactions containing 2 ng of cDNA or PCR standards ranging from 100 to  $1 \times 10^8$  copies, along with SYBR Green I Master mix and primers to quantify different transcripts of interest and were run on a LightCycler® 480 (Roche). Transcript numbers were quantified by comparison to the standard curve using the absolute quantification method and relative expression was determined by comparing to a housekeeping gene, *ACTB*.

For RNA-seq, total RNA was purified using TRIzol® and mRNAs were isolated using the NEBNext Poly(A) mRNA isolation module (New England Biotechnology, E7490L). mRNAs were fragmented by heating to 95°C for ten minutes in a thermocycler and then libraries were generated using the NEBNext® Ultra™ Directional RNA Library Prep Kit for Illumina® (New England Biotechnology, E7420L). Multiplexed libraries were pooled in equimolar ratios and were purified from a 2% TAE-agarose gel prior to sequencing to a length of 50 bases using an

Illumina HiSeq2500. Triplicate samples were analyzed for each drug treatment and analyzed as described in the Bioinformatics section.

***Immunofluorescence, BrdU labelling, TUNEL staining and microscopy***

SU-DIPGXIII or SU-DIPGVI cells were plated on laminin coated coverslips, treated with DMSO, compound 7, etinosat, or Corin for 6-8 days, fixed with 4% PFA for 10 minutes prior to staining. After washing in PBST (PBS + 0.1% Tween20) to remove excess fixative, cells were then permeabilized with 0.25% TritonX-100 in PBS for 30 minutes and blocked in PBST containing 10% serum and 1% BSA. Coverslips were then incubated in block containing dilutions of the following primary antibodies overnight at 4°C: LSD1 (1:500, Abcam, ab17721) NP2 (1:500, Santa Cruz Biotechnology, sc-166035), Ki67 (1:1000, DAKO, M7240), O4 (1:100, a kind gift from Dr. Stefanie Giera), CALB1 (1:500), or Anti- $\beta$ -Tubulin, clone AA2 (1:1,000, EMD Millipore, 05-661). After washing extensively in PBST, the coverslips were incubated with Alexa-fluor conjugated secondary antibodies (Thermo Fisher Scientific) for 30 minutes at room temperature, and then washed extensively in PBS with 0.1% Tween-20 before counterstaining DNA with Hoechst and mounting with Prolong Gold (Thermo Fisher Scientific, P36390) on glass slides. For BrdU staining, 200,000 SU-DIPGVI or SU-DIPGXIII cells were plated on laminin-coated coverslips in 12-wells and treated with DMSO, or 0.5  $\mu$ M compound 7, etinostat, or Corin for three days. 0.03 mg/mL BrdU diluted in growth medium was introduced for 30 minutes before the cells were fixed with 100% ice cold methanol and stained with mouse anti-BrdU (1:1000, Bu20A, Cell Signaling Technology) using HCl to denature the DNA and following the protocol provided by the manufacturer.



### ***Flow cytometry analysis of cell cycle***

One million DIPGXIII cells were treated with DMSO, or 0.5  $\mu$ M compound 7, etinostat, or Corin for 3 days. Neurospheres were disassociated, washed in ice cold PBS, and re-suspended in PBS containing RNAase and Propidium iodide (Sigma, P4170) before analyzing DNA content on a FACSCanto Analyzer (BD Biosciences). Cell cycle analysis was conducted with FlowJo using the Dean-Jett Fox Model.

### ***Analysis of ChIP-seq and RNA-seq datasets***

ChIP-seq experiments to determine changes in chromatin modification in response to the two treatments (DMSO and Corin) were performed in duplicate for each of the analyzed histone marks (H3K4me1, H3K27ac, and H3K27me3) and sequenced using the Illumina platform. FASTQ files were trimmed using Trimmomatic or TrimGalore! (Bolger et al., 2014, [http://www.bioinformatics.babraham.ac.uk/projects/trim\\_galore/](http://www.bioinformatics.babraham.ac.uk/projects/trim_galore/)) and then aligned to hg19 using Bowtie2 (Langmead and Salzberg, 2012). Peaks were called using MACS2 (Zhang et al., 2008) using the “narrow peaks” setting for H3K4me1 (FDR < 0.05) and the “broad peaks” setting for H3K27ac, H3K27me3, and H3K27M (FDR<0.1). ChIP peaks that were significantly increased or decreased in the presence of Corin for both replicates were then identified using the DiffBind package in R (Rory Stark<Rory.Stark@Cruk.Cam.Ac.Uk>, 2017). To visualize ChIP-seq data, aligned BAMs from replicate ChIP experiments were combined using the MergeSamFiles tool using the Picard package (<http://broadinstitute.github.io/picard/>). The bamCoverage function in deepTools (Ramírez et al., 2016) was then used to generate bigwig files for visualization normalizing to 1 $\times$  coverage of hg19 ignoring PCR duplicates and representative track diagrams were generated using Integrated Genomics Viewer software (Robinson et al., 2011). Silenced

and activated chromatin clusters were identified using kmeans clustering analysis in deepTools with an input peak set consisting of all of the differential H3K4me1, H3K27ac, and H3K27me3 peaks identified as described above.

Regions in either the “Corin-silenced” or “Corin-activated” chromatin clusters were associated with different genomic elements using the Cis-regulatory Element Annotation System (CEAS) (Ji et al., 2006) in the Cistrome data analysis pipeline (Liu et al., 2011), defining a promoter as up to 2000 base pairs upstream from the transcription start site and a downstream region up to 1000 base pairs 3' to the transcription end site. Enriched transcription factor motifs were identified using PSCANChIP (Zambelli et al., 2013). REST binding sites were derived from published U87 ChIP-seq data as described in the Key Resource Table. To identify super enhancer-like elements with high H3K27me3 and H3K27ac in the Corin treated samples we first combined the aligned BAM files from H3K27me3 and H3K27ac chIP duplicates using Samtools merge function (Li et al., 2009). We then used the Ranking of Super Enhancers program (ROSE) to first identify distal peaks, then merge adjacent peaks, and finally rank them by their level of H3K27ac or H3K27me3 signal (Whyte et al., 2013). The two nearest genes to each of these enhancer-like elements within 100 kilobases were obtained using the Genomic Regions Enrichment of Annotations Tool (GREAT) (McLean et al., 2010).

To analyze RNA-seq data, raw RNA-seq reads were selected for quality and length using Trimmomatic (Bolger et al., 2014) and then aligned to hg19 using STAR (Dobin et al., 2013). Count tables were generated using featureCounts in the Subread package (Liao et al., 2014) and the resulting count tables were analyzed in R using DESeq2 to identify differentially expressed genes. Genes that were up- or down-regulated at least two fold with an FDR<0.01 were considered differentially expressed for downstream analysis. PCA analysis was performed using

the DESeq2 package in R. After identifying differentially expressed genes, we performed Gene Ontology analyses (Ashburner et al., 2000) using the Bonferroni correction for multiple hypothesis testing to identify gene categories that were up- and down-regulated by the various treatments limiting the outputs shown in the paper to gene sets containing less than 2,500 genes.

### ***Analysis of patient RNA-seq and microarray data***

To determine whether Corin-dependent gene expression changes were associated with genes differentially expressed in normal brain and DIPG samples, we first curated a set of gene expression signatures associated with DIPG from the literature (Pathania et al., 2017; Paugh et al., 2011; Saratsis et al., 2014) (GSE95277 and GSE26576), identified genes that were over- or under-expressed in DIPG versus normal brain samples where necessary. We then performed gene set enrichment analyses (GSEA) (Subramanian et al., 2005) in order to compare a pre-ranked list of genes that were differentially expressed in Corin- versus DMSO-treated SU-DIPGXIII cells to the gene sets that were up- or down-regulated in DIPG samples compared to normal brain.

To assess whether any gene signatures related to LSD1/HDAC inhibition correlated with DIPG patient survival, we analyzed RNA-seq data from a cohort of primary DIPG tumors ([EGAD00001000793](#)). Raw RNA-seq reads were selected for quality and length using TrimGalore! and then aligned to hg19 using the STAR (Dobin et al., 2013). We then generated count tables using featureCounts in the Subread package (Liao et al., 2014). When multiple sequencing samples were available from the same donor they were considered as individual replicates in the downstream analyses and not averaged. To determine if any genes were differentially expressed in tumors expressing “high” and “low” levels of *LSD1* transcripts we

first divided these tumors based on the mean normalized counts for *LSD1* (*KDM1A*) and then identified differentially expressed genes using DeSEQ2 in R (FDR<0.01, fold change 2). When then used gene ontology analysis to find if any gene categories were up- or down-regulated in the RNAseq datasets based on *LSD1* “high” and “low” expression status.

To determine whether the Corin-dependent gene signature correlated with survival time, we first divided the DIPG tumor samples based on the mean survival time and generated Kaplan Meier curves in Graphpad Prism. We then used a log rank test to confirm the statistically significant difference in survival time in the “increased survival” and “decreased survival” groups. As described above, we again used DESeq2 in R to identify genes that were differentially expressed based on survival group (FDR<0.05 and fold change 2). Finally, we performed a pre-ranked GSEA analysis to ask whether the genes that were differentially expressed in the Corin-treated SU-DIPGXIII cells correlated with the genes that were over- or under-expressed in the increased and decreased survival groups. Heatmaps showing the relative differences in gene expression under different conditions were generated in R using the pheatmap package.

## **QUANTIFICATION AND STATISTICAL ANALYSIS**

Sample size for experiments was not pre-determined. Cell viability curves for the different inhibitors were calculated from at least two independent experiments with biological triplicates for each condition. For mouse experiments, animals were randomized into Corin and vehicle treatment groups. Graphs showing changes in Trypan Blue positive cells, TUNEL positive cells, and cells stained with various immunofluorescent markers summarize at least three independent experiments with at least 200 cells scored per condition per stain. Data showing quantification of

transcripts by RT-PCR were similarly derived from at least two independent experiments. Statistical significance was determined by ANOVA, Student's T tests, or the log rank test using Graphpad Prism, or R as described in the figure legends.

## **DATA AND SOFTWARE AVAILABILITY**

Software tools used in this study and links to previously published datasets can be found in the Key Resource Table. Unprocessed mass spectrometry files (.RAW format) for histone PTM analysis are deposited in Harvard Dataverse (<https://dataverse.harvard.edu/>) with the identifier: doi:10.7910/DVN/HCIXPN and available to download. ChIP-seq and RNA-seq data can be found in the Gene Expression Omnibus at NCBI (GSE110572, <https://www.ncbi.nlm.nih.gov/geo/query/acc.cgi?acc=GSE110572>) and then entering the token: crelmksghtitfqv.

## **Author Contributions**

J.N.A., M.G.F. and Y.S. designed and conceived the experiments and wrote the manuscript. J.N.A., B.M.Z., M.K., R.G., M.A.B., S.G., S.M.G., M.W., S.N., R.A., M.L.S., and B.E.B. performed the experiments and analyzed the data. J.N.A., S.M.G. and B.M.Z., generated and analyzed the NGS and mass spectrometry data. J.N.A., D.M.B, Q.D., M.G.F., and T.R.G. designed and conducted the mouse xenograft experiments and tissue analysis. S.A. performed the histopathological analysis and quantification. J.H.K., J.D., and P.A.C. designed and synthesized small molecules used in these studies.

## **Acknowledgments**

We thank Dr.'s Michelle Monje, Keith Ligon, Nada Jabado, Jaume Mora, Angel Montero Carcaboso, and Hongwu Zheng for generously providing cell lines and for their helpful advice on experiments. We also thank Dr. Roderick Bronson, and the Harvard Medical School Rodent Histopathology Core for their assistance with histopathology experiments and interpretation and Ross Tomaino of the Taplin Mass Spectrometry Facility for assistance with histone proteomic experiments. This work was supported by generous funding from The Cure Starts Now, The DIPG Collaborative, the National Cancer Institute (R35 CA210104-01) and Boston Children's Hospital to Y.S. J.N.A. was supported by a Ruth L. Kirchstein Fellowship from the National Cancer Institute (F32 CA189741-01), the Rally Foundation for Pediatric Cancer Research, Vs. Cancer, the Defeat DIPG/Mark Mosier Foundation and the Chad Tough Foundations. M.G.F. holds a Career Award for Medical Scientist from Burroughs Wellcome Fund and is supported by the N.I.H. (3P30 CA006516-53S6), The Cure Starts Now Foundation, Solving Kids' Cancer, Inc/The Bibi Fund, The Andruzzi Foundation, and Alex's Lemonade Stand Foundation. M.K. was supported by the Harvard College Research Program for undergraduate research. R.G. was supported by the Harvard Program in Neonatology Summer Student Research Program. J.H.K., J.D., and P.A.C. were supported by N.I.H. (F32GM108364, R37GM62437) as well as the V Foundation, the FAMRI Foundation, and the Leukemia and Lymphoma Society. Y.S. is an American Cancer Society Research Professor.

## **Declaration of Interests**

Y.S. is a consultant/Advisor for the Institutes of Biomedical Sciences, Fudan University, Shanghai Medical School. YS is a co-founder and equity holder of Constellation Pharmaceuticals, Inc, a consultant and an equity holder of Guangzhou BeBetter Medicine Technology Co., LTD and an equity holder of Imago Biosciences. B.E.B. is an advisor and equity holder for Fulcrum Therapeutics, HiFiBio and Arsenal Biosciences, is an advisor for Cell Signaling Technologies, and has equity in Nohla Therapeutics, BioMillenia and 1CellBio. T.R.G. serves as an advisor to Foundation Medicine, Glaxo Smith Kline, and Sherlock Biosciences. A U.S. patent application including Corin as a novel chemical entity has been filed with J.H.K. and P.A.C as inventors.

## FIGURE LEGENDS

### **Figure 1: The bifunctional LSD1i and HDACi, Corin inhibits DIPG growth and induces global changes in covalent histone modifications.**

(A) Heatmap summarizing the  $Ic_{50}$  values calculated after treating NHA-hTERT, SU-DIPGIV, SU-DIPGXIII, or SU-DIPGVI cells with increasing doses of small molecule inhibitors targeting various epigenetic regulators with n/a indicating conditions where an  $Ic_{50}$  could not be determined.

(B)-(E) Average percent cell viability of (B), SU-DIPGVI, (C), SU-DIPGXIII, (D), BT869 and (E), NHA-hTERT cells following treatment with dose curves of compound 7 (LSD1i), etinostat (HDACi), or the dual inhibitor, Corin showing further growth inhibition when HDACs and LSD1 are co-inhibited in K27M mutant SU-DIPGVI, SU-DIPGXIII, and BT869 cells but not in non-transformed NHA-TERTs.

(F) Average cell viability of non-transformed BJ fibroblasts (black curve) compared to H3K27M mutant DIPG cell lines (HSJD-DIPG007 and BT245, purple curves). Data in panels (B)-(F) are from at least two independent experiments with biological triplicates with error bars indicating the S.E.M.

(G)-(J) Histograms summarizing the fold change in abundance of various histone tail peptides purified from SU-DIPGXIII cells treated with 0.5  $\mu$ M compound 7, etinostat, or Corin compared to DMSO. Error bars indicate the standard deviation calculated from three experiments comparing Corin and DMSO-treated samples and statistical significance was determined using an un-paired Student's T test with  $*p<0.05$ ,  $**p<0.001$ , and  $***p<0.0001$ .



(K) Western blots of SU-DIPGXIII lysates collected 7 days after beginning treatment with 0.5  $\mu$ M of the indicated compounds incubated with antibodies to detect covalent histone modifications.

(L)-(N) Analysis of HSJD-DIPG007 response to Corin treatment for either 2 or 6 days to assess the levels of histone marks by Western blotting (H3K4me1, H3K27ac, H3K27me3) compared to loading controls (ACTIN and total H3), (L), the corresponding percent Trypan Blue (+) dead or dying cells, (M), and the overall number of viable cells, (N). Due to inconsistent lysate quality resulting from poor cell viability, corresponding Western blots are not available from DIPG007 cells treated with 1.0  $\mu$ M Corin for 6 days. In (M)-(N) statistical significance was determined using a one way ANOVA comparing all column means to DMSO with  $*p<0.05$ ,  $**p<0.01$ , and  $***p<0.001$ .

**Figure 2: Dual inhibition of LSD1 and HDACs alters the chromatin landscape in DIPG.**

(A) Heatmaps of ChIP-seq profiles from SU-DIPGXIII cells showing the top 5,000 H3K27M peaks (top panel), or the regions where treatment with 0.5  $\mu$ M Corin induced a more activated chromatin signature marked by increased H3K4me1 and H3K27ac (“Corin-activated,” middle panels), or where Corin induced a more “silenced” chromatin profile marked by increased H3K27me3 (“Corin-silenced,” bottom panel).

(B) Average ChIP-seq signal for H3K27M (first column), H3K27ac (second column), H3K4me1 (third column), and H3K27me3 (fourth column) centered around the K27M-bound, the “Corin-activated,” and the “Corin-silenced” peak sets shown in panel, (A).

(C) Pie charts showing the overlap between Corin-activated genomic regions (increased H3K27ac and H3K4me1), Corin-silenced chromatin regions (increased H3K27me3), and K27M-bound regions and various genomic elements.

(D) Heatmap showing the  $-\log_{10} p$ -values for the enrichment of various transcription factor binding motifs in Corin-activated and Corin-silenced chromatin regions from panels (A) and (B).

(E) REST transcription factor binding motif found to be enriched in the set of genomic regions where Corin induced an activated chromatin state.

(F) Integrated genomics viewer screenshot of the *CELSRI* gene locus showing mapped sequencing reads from chromatin immunoprecipitated with antibodies targeting H3K27M, H3K4me1, H3K27ac, and H3K27me3 from DMSO- and Corin-treated SU-DIPGXIII cells showing localized increases in H3K27ac and H3K4me1 at REST motifs.

**Figure 3: Dual inhibition of LSD1 and HDACs with Corin synergistically alters gene expression in DIPG.**

(A)-(C) Volcano plots showing the  $-\log_{10} (p\text{-values})$  and  $\log_2$  fold change for transcripts detected by RNA-seq from SU-DIPGXIII cells treated for 7 days with (A), 0.5  $\mu\text{M}$  Compound 7, (B), 0.5  $\mu\text{M}$  etinostat, or (C), 0.5  $\mu\text{M}$  Corin. Significant genes ( $adj\ p < 0.01$ ) with at least a 2 fold change over DMSO are marked in magenta (up-regulated), or blue (down-regulated).

(D) PCA analysis of RNA-seq datasets generated from SU-DIPG-XIII cells treated with the different compounds at 0.5  $\mu\text{M}$ .

(E)-(F) Venn diagrams illustrating the overlap between genes that were either up-, (E), or down-regulated, (F), in response to drug treatment, revealing a large number of transcripts uniquely regulated by Corin.

(G) Metagene plots showing the average ChIP signal for H3K4me1, H3K27ac, and H3K27me3 for all of the Corin up-regulated genes (left panels), and down-regulated genes (right panels).

(H)-(I) Ranking of H3K27ac and H3K27me3 ChIP peaks that were increased in the presence of Corin to identify strongly activated, and strongly inhibited enhancer elements, respectively.

Select genes that were up- or down-regulated by Corin found within 100 Kb are labelled with asterisks.

(J) Representative Western blots analyzing lysates from SU-DIPGXIII cells that were treated with either vehicle for 24 or 48 hours or with 0.5  $\mu$ M Corin for 1, 2, 4, 8, 24, or 48 hours to monitor the level of H3K27ac over a short time course with an actin blot serving as a loading control.

(K)-(L) RT-PCR analysis of two Corin-target genes (*NEFL* and *SEMA3C*) in cDNA generated from SU-DIPGXIII samples collected after treatment with a time course of Corin corresponding with the Western blots in panel, (J).

**Figure 4: Dual inhibition of LSD1 and HDACs with Corin induces differentiation in DIPG.**

(A) Gene ontology analysis of genes up-regulated in SU-DIPGXIII cells due to treatment with the various inhibitors revealing an enrichment in genes associated with neuronal differentiation and developmental processes in the Corin-treated samples.

(B)-(C) Summary of quantitative RT-PCR results confirming the up-regulation of markers associated with neural differentiation, (B), or the down-regulation of transcripts associated with neuronal and oligodendrocyte progenitors, (C), after SU-DIPGXIII cells were treated with 0.5  $\mu$ M compound 7, etinostat or Corin for 7 days. Statistical significance was determined using a

one-way ANOVA comparing all means to DMSO with  $*p<0.05$ ,  $**p<0.01$  and  $***p<0.001$ , and n.s. indicating non-significant results.

(D)-(F) Summary of RT-PCR data analyzing changes in the expression of differentiation markers, (D)-(E), or the progenitor marker, *CSPG4*, (F), in additional DIPG cells that were treated with 0.25  $\mu$ M Corin for 6 days (HSJD-DIPG007, BT869, SU-DIPGXIII\*), or for 8 days (BT245). In panels (D)-(F) statistical significance was determined using an un-paired Student's T test with  $*p<0.05$ ,  $**p<0.01$  and  $***p<0.001$ , and n.s. indicating non-significant results.

(G) Representative immunofluorescence images of SU-DIPGXIII cells that were plated on laminin, and treated with either DMSO or Corin for 7 days before staining with antibodies to the Corin-targets, NP2 (left panels), and CALB1 (right panels). Scale bars are 50  $\mu$ m.

(H) Immunofluorescence images of SU-DIPGXIII cells grown on laminin in the presence of the indicated compounds prior to staining them with anti- $\beta$ -tubulin to reveal neurite-like extensions (marked by white arrowheads). Scale bar is 20  $\mu$ m.

(I) Bright field images of SU-DIPGVI neurospheres treated with various compounds showing the induction of neurites in spheroids treated with etinostat or Corin, with a more pronounced phenotype observed in the Corin-treated cells. Scale bar is 100  $\mu$ m.

### **Figure 5: Dual inhibition of LSD1 and HDACs results in cell cycle arrest in DIPG.**

(A) Summary of top enriched GO categories in gene sets that were down-regulated in SU-DIPGXIII cells due to treatment with different inhibitors, suggesting that Corin inhibits the expression of genes involved in cell cycle progression.

(B)-(C) Average expression of two cell cycle regulators (*CCNB1* and *AURKB*) in SU-DIPGXIII and SU-DIPGVI cells after one-week treatment with the indicated compounds.

(D) Analysis of *AURKB* and *CCNBI* expression in additional DIPG cell lines (BT245, BT869, HSJD-DIPG007, and SU-DIPGXIIIP\*) after 6-8 days treatment with 0.25  $\mu$ M Corin or DMSO.

In panels (B)-(D) error bars show S.E.M. and statistical significance was determined using an un-paired Student's T test with  $*p<0.05$ ,  $**p<0.01$  and  $***p<0.001$ , and n.s. indicating non-significant results. Scale bars are 20  $\mu$ m.

(E)-(F) Representative images of SU-DIPGVI cells on laminin coated plates that were pulsed with BrdU for 30 minutes and then stained with anti-BrdU to detect S-phase nuclei (red), (E), which were quantified in (F), which also includes data from SU-DIPGXII cells. Scale bars are 20  $\mu$ m.

(G)-(H) Representative images of Ki67-stained SU-DIPGXIII cells, (G), and quantification, (H) after 7 days treatment with 0.5  $\mu$ M Corin, or DMSO. In panels (F) and (H) statistical significance was determined using a Student's T-test with  $*p<0.05$ ,  $***p<0.001$ .

**Figure 6: Corin treatment reduces DIPG xenograft size and alters tumor phenotypes.**

(A) Representative bioluminescent images of mice xenografted with HSJD-DIPG007+luciferase/Zs-green cells immediately prior to, or 7 days after treatment with 0.03 mg Corin or saline control administered by CED.

(B) Average luciferase signal (BLI) from HSJD-DIPG007 xenografts taken either prior to treatment or 7 days after treatment with either saline or Corin.

(C) Average BLI signal from SU-DIPGXIIIP\* xenografts taken at various time points before and after CED (teal arrow) with either 0.03 mg Corin or DMSO. In (B)-(C) error bars show S.E.M. and statistical significance was determined by ANOVA using the Benjamini, Krieger and Yekutieli method to correct for multiple comparisons.

(D) Hematoxylin-eosin (H&E) stained sections at the level of the pons showing growth of high-grade glioma at the site of injection of patient-derived SU-DIPGXIIIP\* cells (top left, x20) characterized by palisading necrosis, marked atypia and mitoses (bottom left, x400). There is almost complete necrosis (geographic pattern) of the tumor at the site of Corin injection, surrounded by degenerating tumor cells with nuclear debris (top right panels, x20). Intermingled occasional tumor cells are seen surrounding the area of necrosis, but these are at a significantly lower density than in the untreated tumors (bottom right panel, x400).

(E) Representative images of mouse brains harboring SU-DIPGXIIIP\* pontine xenografts collected 3 days after treatment with either vehicle or Corin that were stained with antibodies to monitor H3K27ac and H3K27me3 levels. The top panels show images of normal mouse brain in the pons adjacent to the tumors and the bottom panels show regions of the SU-DIPGXIIIP\* xenograft tumors. Scale bar is 50  $\mu$ m.

(F) Representative images of sections of SU-DIPGXIIIP\* xenografts after treatment with either vehicle (left) or Corin (right) after staining with antibodies to detect the Corin-targets, NP2 (top panels), and SYNI/II/III (bottom panels). Scale bar is 20  $\mu$ m.

(G) Representative immunohistochemistry for Ki67 to mark proliferative cells (top two panels) and cleaved Caspase-3 to mark apoptotic cells (cCaspase3, bottom panels) in SU-DIPGXIIIP\* xenografts from vehicle- and Corin-treated mice. Scale bars are 20  $\mu$ m.

**Figure 7: Corin-dependent gene signatures are associated with favorable prognosis in DIPG patient datasets.**

(A) Scatter plot of *LSD1* expression in patient DIPG tumors from the St. Jude cohort (see STAR methods) divided into “low” and “high” subgroups based on the median expression of *LSD1*.

\*\*\* $p < 0.001$  by Student’s T-test.

(B) Summary of  $-\log_{10}$  Bonferonni corrected  $p$ -values associated with the top six most-enriched GO categories in the *LSD1* high-expressing compared to the *LSD1* low-expressing DIPG tumor subsets from panel, (A) revealing an enrichment in gene sets associated with cell division and mitosis in DIPG samples with “high” *LSD1* expression.

(C) Pre-ranked GSEA analysis of Corin-dependent gene expression changes in SU-DIPGXIII RNAseq datasets compared to genes that are over- (leftmost three panels) or under-expressed (rightmost two panels) in DIPG tumor samples compared to normal brain.

(D) Kaplan Meier survival curves generated from RNA-seq data from the St. Jude patient cohort who were diagnosed with DIPG separated into decreased and increased survival groups.

Statistically significant differences in survival were determined using a log-rank test.

(E) Pre-ranked GSEA analysis of Corin-dependent gene expression changes in SU-DIPGXIII RNAseq datasets revealing that Corin results in a significant up-regulation of genes associated with increased survival in DIPG in the St. Jude cohort.

(F) Heatmaps summarizing the  $\log_2$  fold change in expression for genes that were up-regulated in DIPG tumor samples from patients with increased survival (right panel), or that were similarly up-regulated in SU-DIPGXIII cells treated with Corin (left panel).

**Figure S1, related to Figure 1**

**A CRISPR/Cas9 dropout screen identifies modulators of SU-DIPGVI sensitivity to HDAC inhibition.**

(A) Schematic of CRISPR screen to find HDACi synergizers in DIPG.

(B) Histograms summarizing flow cytometry-based analysis of parental SU-DIPGVI (left) or Cas9-transduced (SU-DIPGVI) cells expressing a GFP-based reporter of Cas9-dependent gene editing. The percent of GFP+ cells (indicative of failed Cas9-dependent gene editing) was decreased by ~60% in the Cas9-expressing SU-DIPG-VI cells three weeks post-infection (compare top and bottom panels).

(C) Growth curves of SU-DIPGVI cells grown in either regular media, media containing DMSO (vehicle control), or increasing doses of panobinostat.

(D)-(E) Scatter plots showing statistically significant correlations in sgRNA abundance determined by next generation sequencing from biological replicates of SU-DIPGVI cells grown for (D), 3 additional weeks after the reference samples were taken in control media, or (E), 3 additional weeks after the reference samples were taken in media containing 1.25 nM panobinostat.

(F) Scatter plot summarizing  $-\log_{10} p$ -values for each of the genes in the CRISPR screen with hits shown in purple.

(G)-(J) Representative immunofluorescent images of endogenous LSD1 levels in SU-DIPGVI+Cas9 cells, (G), or HSJD-DIPG007+Ca9 cells, (I), that were infected with Control or LSD1 sgRNAs prior to treatment with etinostat, panobinostat, or Corin. Cell nuclei with low/un-detectable levels of LSD1 are indicated by white arrowheads and quantified in panel, (H) for SU-DIPGVI cells and panel, (J) for HSJD-DIPG007 cells.



**Figure S2, related to Figure 1**

**Co-treatment with HDAC and LSD1 inhibitors synergistically reduces DIPG viability.**

(A) Chemical structures of the LSD1i, compound 7, the dual LSD1 and HDACs1-3 inhibitor, Corin, and compound 9, a Corin analog that cannot inhibit LSD1.

(B) Average cell viability determined using Cell TiterGlo of SU-DIPG-XIII (left), SU-DIPGVI (center), and NHA-hTERT (right) cells following treatment with combinations of compound 7, and panobinostat.

(C) Heatmaps showing the percent growth inhibition of SU-DIPGVI (left) and SU-DIPGXIII cells treated with increasing doses of compound 7 and etinostat suggesting a synergistic relationship between these compounds with BLISS scores of 9.36 and 2.00, respectively.

(D) Contour plot used to calculate synergy by BLISS analysis of SU-DIPGVI responses to combinations of etinostat and compound 7.

(E) Average viability of BT245 and HSJD-DIPG007 cells after one week treatment with the indicated compounds suggesting stronger inhibition of growth with the dual LSD1/HDAC inhibitor Corin than individual HDAC and LSD1 inhibitors (etinostat, and compound 7), but no advantage provided by a Corin-analog that cannot inhibit LSD1 (compound 9) over the HDACi alone.

(F) Average cell viability of SU-DIPGXIII cells after treatment with various compound combinations for one week showing a similar extent of growth inhibition with Corin treatment or with equimolar levels of compound 7 and etinostat.

(G) Number of viable SU-DIPGVI+Cas9 cells expressing either Control sgRNA (white bars) or LSD1 sgRNA (black bars) following treatment with the indicated compounds.

(H) Average percent trypan blue (+) SU-DIPGVI cells (left) after 24 hours of treatment with a 1  $\mu$ M dose of the indicated compounds, or percent Trypan Blue (+) SU-DIPGXIII cells (right) after treatment with an 0.5  $\mu$ M dose of the indicated compounds determined from three independent experiments.

(I) Representative fluorescent images of SU-DIPGVI cells that were plated on laminin-coated coverslips prior to treatment with either DMSO or 1  $\mu$ M of Corin for 24 hours prior to TUNEL staining. Scale bar is 10  $\mu$ m.

(J) Quantification of the average number of TUNEL+ SU-DIPGVI cells as in, (H) as an indicator of apoptosis. Statistical significance in panels (H) and (J) was determined using an un-paired Student's T test, while statistical significance in panel (G) was determined using a one-way ANOVA comparing all the means with  $p < 0.05^*$ ,  $**p < 0.01$ ,  $***p < 0.001$ .

**Figure S3, related to Figure 1 and 2.**

**Corin treatment results in global changes in the covalent modification of DIPG chromatin.**

(A) Histogram summarizing the log<sub>2</sub> fold change in the abundance of various modified histone peptides from SU-DIPGXIII cells treated for 7 days with DMSO, compound 7 (red dots), etinostat (blue dots), or Corin (lavender columns). Statistical significance was determined using a Student's T test with  $p < 0.05^*$ ,  $**p < 0.01$ ,  $***p < 0.001$ .

(B) Heatmap summarizing the log<sub>2</sub> fold change in the abundance of various modified histone peptides from SU-DIPGVI or SU-DIPGXIII cells treated with 0.5  $\mu$ M of the indicated compounds.

(C)-(E) Analysis of SU-DIPGXIII\* cell response to Corin treatment for either 2 or 6 days to assess the levels of histone marks by Western blotting (H3K4me1, H3K27ac, H3K27me3)

compared to loading controls (ACTIN and total H3), (C), the corresponding percent Trypan Blue (+) dead or dying cells, (D), and the overall number of viable cells, (E). Due to inconsistent lysate quality resulting from poor cell viability, corresponding Western blots are not available from SU-DIPGXIII\* cells treated with 1.0  $\mu$ M Corin for 6 days. In (D)-(E) statistical significance was determined using a one way ANOVA comparing all column means to DMSO with \* $p$ <0.05, \*\* $p$ <0.01, and \*\*\* $p$ <0.001.

(F) Average SU-DIPGXIII ChIP-seq profiles for H3K4me1, H3K27ac, and H3K27me3 centered around REST binding sites from ENCODE REST ChIP-seq data generated from U87-MG human glioblastoma cells (Gene expression omnibus, [GSM803372](#)).

**Figure S4, related to Figure 1 and 2.**

**Histone mutation status is not sufficient to predict sensitivity to Corin.**

(A) Western blots of lysates from NHA-hTERT (right panels) and *tp53*<sup>-/-</sup> murine neural stem cells (mNSCs *tp53*<sup>-/-</sup>) (left panels) overexpressing either flag-H3.3 WT or flag-H3.3 K27M mutant histones probed to detect flag, H3K27me3, total H3 and ACTIN.

(B)-(C) Average viability of NHA-hTERT, (C), and mNSCs *tp53*<sup>-/-</sup> expressing various flag-tagged histone proteins after one week treatment with increasing doses of Corin.

**Figure S5, related to Figure 6.**

**Analysis of SU-DIPGXIII xenografts treated with vehicle or Corin by convection enhanced delivery.**

(A) Hematoxylin-eosin (H&E) stained sections images of hindbrain sections from mice xenografted with HSJD-DIPG007+luciferase/Zs-green cells that were treated with DMSO or 0.03 mg of Corin by CED.

(B) Hematoxylin-eosin (H&E) stained sections of hindbrain (top) and midbrain (bottom) sections from mice xenografted with SU-DIPGXIII\*+luciferase/Zs-green cells showing a large tumor mass in the pons at the site of injection (top panel) as well as extensive leptomeningeal spread. In (A)-(B) scale bars are 1 mm.

(C) Representative Hoechst-stained sections of mouse hindbrains that were xenografted with SU-DIPGXIII cells (yellow arrowheads) in the pons collected two weeks after convection enhanced delivery of either vehicle control (left), or 0.03 mg Corin (right).

(D) Quantification of the percent of tumor nuclei in mice xenografted with SU-DIPGXIII cells in the pons, treated with vehicle or Corin. A Student's T-test with Welch's correction was used to determine statistical significance with  $*p < 0.05$ .

(E)-(F) Quantification of the mean intensity of H3K27ac, (E), and H3K27me3, (F) staining as shown in Figure 6E. Staining intensity was determined within nuclei as defined by Hoechst staining using CellProfiler.

(G) Representative images of vehicle-treated (top panels) and Corin-treated SU-DIPGXIII\* xenografts stained to detect H3K27ac (left panels) and H3K27me3 (right panels) either the tumor core (center panels) or towards the tumor periphery (bottom panels) away from the putative site of Corin injection. Scale bar is 50  $\mu$ m.

**Table S1:** Ic50 values for epigenetic inhibitors in DIPG cell lines and NHA-hTERTs.

**Table S2:** Summary of gene hits from CRISPR screen for factors that synergize with panobinostat in SU-DIPGVI cells.

**Table S3:** Summary of proteomics datasets analyzing changes in histone modifications.

**Table S4:** Summary of gene expression changes from RNAseq analysis of SU-DIPGXIII cells.

**Table S5:** Summary of gene expression differences in primary DIPG tumors grouped by survival status and LSD1 expression group.

**Table S6:** List of primers and sgRNA sequences used in this study.

## References:

Abrajano, J.J., Qureshi, I.A., Gokhan, S., Molero, A.E., Zheng, D., Bergman, A., and Mehler, M.F. (2010). Corepressor for element-1-silencing transcription factor preferentially mediates gene networks underlying neural stem cell fate decisions. *Proc. Natl. Acad. Sci.* *107*, 16685–16690.

Amente, S., Lania, L., and Majello, B. (2013). The histone LSD1 demethylase in stemness and cancer transcription programs. *Biochim. Biophys. Acta BBA - Gene Regul. Mech.* *1829*, 981–986.

Ashburner, M., Ball, C.A., Blake, J.A., Botstein, D., Butler, H., Cherry, J.M., Davis, A.P., Dolinski, K., Dwight, S.S., Eppig, J.T., et al. (2000). Gene ontology: tool for the unification of biology. The Gene Ontology Consortium. *Nat. Genet.* *25*, 25–29.

Atadja, P., Gao, L., Kwon, P., Trogani, N., Walker, H., Hsu, M., Yeleswarapu, L., Chandramouli, N., Perez, L., Versace, R., et al. (2004). Selective growth inhibition of tumor cells by a novel histone deacetylase inhibitor, NVP-LAQ824. *Cancer Res.* *64*, 689–695.

Ballas, N., and Mandel, G. (2005). The many faces of REST oversee epigenetic programming of neuronal genes. *Curr. Opin. Neurobiol.* *15*, 500–506.

Ballas, N., Grunseich, C., Lu, D.D., Speh, J.C., and Mandel, G. (2005a). REST and Its Corepressors Mediate Plasticity of Neuronal Gene Chromatin throughout Neurogenesis. *Cell* *121*, 645–657.

Ballas, N., Grunseich, C., Lu, D.D., Speh, J.C., and Mandel, G. (2005b). REST and Its Corepressors Mediate Plasticity of Neuronal Gene Chromatin throughout Neurogenesis. *Cell* 121, 645–657.

Bender, S., Tang, Y., Lindroth, A.M., Hovestadt, V., Jones, D.T.W., Kool, M., Zapatka, M., Northcott, P.A., Sturm, D., Wang, W., et al. (2013). Reduced H3K27me3 and DNA hypomethylation are major drivers of gene expression in K27M mutant pediatric high-grade gliomas. *Cancer Cell* 24, 660–672.

Bolger, A.M., Lohse, M., and Usadel, B. (2014). Trimmomatic: a flexible trimmer for Illumina sequence data. *Bioinforma. Oxf. Engl.* 30, 2114–2120.

Boucherie, C., Boutin, C., Jossin, Y., Schakman, O., Goffinet, A.M., Ris, L., Gailly, P., and Tissir, F. (2018). Neural progenitor fate decision defects, cortical hypoplasia and behavioral impairment in *Celsr1*-deficient mice. *Mol. Psychiatry* 23, 723–734.

Carpenter, A.E., Jones, T.R., Lamprecht, M.R., Clarke, C., Kang, I.H., Friman, O., Guertin, D.A., Chang, J.H., Lindquist, R.A., Moffat, J., et al. (2006). CellProfiler: image analysis software for identifying and quantifying cell phenotypes. *Genome Biol.* 7, R100.

Chan, K.-M., Fang, D., Gan, H., Hashizume, R., Yu, C., Schroeder, M., Gupta, N., Mueller, S., James, C.D., Jenkins, R., et al. (2013). The histone H3.3K27M mutation in pediatric glioma reprograms H3K27 methylation and gene expression. *Genes Dev.* 27, 985–990.

Chong, J.A., Tapia-Ramírez, J., Kim, S., Toledo-Aral, J.J., Zheng, Y., Boutros, M.C., Altshuler, Y.M., Frohman, M.A., Kraner, S.D., and Mandel, G. (1995). REST: a mammalian silencer protein that restricts sodium channel gene expression to neurons. *Cell* 80, 949–957.

- Cordero, F.J., Huang, Z., Grenier, C., He, X., Hu, G., McLendon, R.E., Murphy, S.K., Hashizume, R., and Becher, O.J. (2017). Histone H3.3K27M Represses *p16* to Accelerate Gliomagenesis in a Murine Model of DIPG. *Mol. Cancer Res.* *15*, 1243–1254.
- Creyghton, M.P., Cheng, A.W., Welstead, G.G., Kooistra, T., Carey, B.W., Steine, E.J., Hanna, J., Lodato, M.A., Frampton, G.M., Sharp, P.A., et al. (2010). Histone H3K27ac separates active from poised enhancers and predicts developmental state. *Proc. Natl. Acad. Sci. U. S. A.* *107*, 21931–21936.
- Culhane, J.C., Wang, D., Yen, P.M., and Cole, P.A. (2010). Comparative analysis of small molecules and histone substrate analogues as LSD1 lysine demethylase inhibitors. *J. Am. Chem. Soc.* *132*, 3164–3176.
- Dickinson, M., Ritchie, D., DeAngelo, D.J., Spencer, A., Ottmann, O.G., Fischer, T., Bhalla, K.N., Liu, A., Parker, K., Scott, J.W., et al. (2009). Preliminary evidence of disease response to the pan deacetylase inhibitor panobinostat (LBH589) in refractory Hodgkin Lymphoma. *Br. J. Haematol.* *147*, 97–101.
- Dobin, A., Davis, C.A., Schlesinger, F., Drenkow, J., Zaleski, C., Jha, S., Batut, P., Chaisson, M., and Gingeras, T.R. (2013). STAR: ultrafast universal RNA-seq aligner. *Bioinforma. Oxf. Engl.* *29*, 15–21.
- Easwaran, H., Tsai, H.-C., and Baylin, S.B. (2014). Cancer epigenetics: tumor heterogeneity, plasticity of stem-like states, and drug resistance. *Mol. Cell* *54*, 716–727.
- Feng, J., Han, Q., and Zhou, L. (2012). Planar cell polarity genes, *Celsr1-3*, in neural development. *Neurosci. Bull.* *28*, 309–315.



Filippakopoulos, P., Qi, J., Picaud, S., Shen, Y., Smith, W.B., Fedorov, O., Morse, E.M., Keates, T., Hickman, T.T., Felletar, I., et al. (2010). Selective inhibition of BET bromodomains. *Nature* 468, 1067–1073.

Fiskus, W., Sharma, S., Shah, B., Portier, B.P., Devaraj, S.G.T., Liu, K., Iyer, S.P., Bearss, D., and Bhalla, K.N. (2014). Highly effective combination of LSD1 (KDM1A) antagonist and pan-histone deacetylase inhibitor against human AML cells. *Leukemia* 28, 2155–2164.

Fontebasso, A.M., Liu, X.-Y., Sturm, D., and Jabado, N. (2013). Chromatin Remodeling Defects in Pediatric and Young Adult Glioblastoma: A Tale of a Variant Histone 3 Tail: Chromatin Remodeling Defects in Pediatric and Young Adult Glioblastoma. *Brain Pathol.* 23, 210–216.

Gao, Z., Ure, K., Ding, P., Nashaat, M., Yuan, L., Ma, J., Hammer, R.E., and Hsieh, J. (2011). The Master Negative Regulator REST/NRSF Controls Adult Neurogenesis by Restraining the Neurogenic Program in Quiescent Stem Cells. *J. Neurosci.* 31, 9772–9786.

Grasso, C., Tang, Y., Truffaux, N., Berlow, N., Liu, L., Debily, M., Quist, M., Davis, L., Huang, E., Woo, P., et al. (2015). Functionally defined therapeutic targets in diffuse intrinsic pontine glioma. *Nat. Med.* 21, 555–559.

Hakimi, M.-A., Dong, Y., Lane, W.S., Speicher, D.W., and Shiekhata, R. (2003). A candidate X-linked mental retardation gene is a component of a new family of histone deacetylase-containing complexes. *J. Biol. Chem.* 278, 7234–7239.

Harutyunyan, A.S., Krug, B., Chen, H., Papillon-Cavanagh, S., Zeinieh, M., De Jay, N., Deshmukh, S., Chen, C.C.L., Belle, J., Mikael, L.G., et al. (2019). H3K27M induces defective

chromatin spread of PRC2-mediated repressive H3K27me2/me3 and is essential for glioma tumorigenesis. *Nat. Commun.* *10*, 1262.

Hashizume, R., Andor, N., Ihara, Y., Lerner, R., Gan, H., Chen, X., Fang, D., Huang, X., Tom, M.W., Ngo, V., et al. (2014). Pharmacologic inhibition of histone demethylation as a therapy for pediatric brainstem glioma. *Nat. Med.* *20*, 1394–1396.

Hennika, T., Hu, G., Olaciregui, N.G., Barton, K.L., Ehteda, A., Chitranjan, A., Chang, C., Gifford, A.J., Tsoli, M., Ziegler, D.S., et al. (2017). Pre-Clinical Study of Panobinostat in Xenograft and Genetically Engineered Murine Diffuse Intrinsic Pontine Glioma Models. *PLOS ONE* *12*, e0169485.

Jambhekar, A., Anastas, J.N., and Shi, Y. (2017). Histone Lysine Demethylase Inhibitors. *Cold Spring Harb. Perspect. Med.* *7*, a026484.

Jansen, M.H.A., van Vuurden, D.G., Vandertop, W.P., and Kaspers, G.J.L. (2012). Diffuse intrinsic pontine gliomas: A systematic update on clinical trials and biology. *Cancer Treat. Rev.* *38*, 27–35.

Ji, X., Li, W., Song, J., Wei, L., and Liu, X.S. (2006). CEAS: cis-regulatory element annotation system. *Nucleic Acids Res.* *34*, W551-554.

Jiao, L., and Liu, X. (2015). Structural basis of histone H3K27 trimethylation by an active polycomb repressive complex 2. *Science* *350*, aac4383.

Jin, X., Kim, L.J.Y., Wu, Q., Wallace, L.C., Prager, B.C., Sanvoranart, T., Gimple, R.C., Wang, X., Mack, S.C., Miller, T.E., et al. (2017). Targeting glioma stem cells through combined BMI1 and EZH2 inhibition. *Nat. Med.* 23, 1352–1361.

Johnson, R., Teh, C.H., Kunarso, G., Wong, K.Y., Srinivasan, G., Cooper, M.L., Volta, M., Chan, S.S., Lipovich, L., Pollard, S.M., et al. (2008). REST Regulates Distinct Transcriptional Networks in Embryonic and Neural Stem Cells. *PLoS Biol.* 6, e256.

Johung, T.B., and Monje, M. (2017). Diffuse Intrinsic Pontine Glioma: New Pathophysiological Insights and Emerging Therapeutic Targets. *Curr. Neuropharmacol.* 15, 88–97.

Jones, C., and Baker, S.J. (2014). Unique genetic and epigenetic mechanisms driving paediatric diffuse high-grade glioma. *Nat. Rev. Cancer* 14.

Jones, C., Karajannis, M.A., Jones, D.T.W., Kieran, M.W., Monje, M., Baker, S.J., Becher, O.J., Cho, Y.-J., Gupta, N., Hawkins, C., et al. (2016). Pediatric high-grade glioma: biologically and clinically in need of new thinking. *Neuro-Oncol.* now101.

Juratli, T.A., Qin, N., Cahill, D.P., and Filbin, M.G. (2017). Molecular pathogenesis and therapeutic implications in pediatric high-grade gliomas. *Pharmacol. Ther.*

Justin, N., Zhang, Y., Tarricone, C., Martin, S.R., Chen, S., Underwood, E., De Marco, V., Haire, L.F., Walker, P.A., Reinberg, D., et al. (2016). Structural basis of oncogenic histone H3K27M inhibition of human polycomb repressive complex 2. *Nat. Commun.* 7, 11316.

Kalin, J.H., Wu, M., Gomez, A.V., Song, Y., Das, J., Hayward, D., Adejola, N., Wu, M., Panova, I., Chung, H.J., et al. (2018). Targeting the CoREST complex with dual histone deacetylase and demethylase inhibitors. *Nat. Commun.* 9, 53.

Khuong-Quang, D.-A., Buczkowicz, P., Rakopoulos, P., Liu, X.-Y., Fontebasso, A.M., Bouffet, E., Bartels, U., Albrecht, S., Schwartzentruber, J., Letourneau, L., et al. (2012). K27M mutation in histone H3.3 defines clinically and biologically distinct subgroups of pediatric diffuse intrinsic pontine gliomas. *Acta Neuropathol. (Berl.)* 124, 439–447.

Kruidenier, L., Chung, C., Cheng, Z., Liddle, J., Che, K., Joberty, G., Bantscheff, M., Bountra, C., Bridges, A., Diallo, H., et al. (2012). A selective jumonji H3K27 demethylase inhibitor modulates the proinflammatory macrophage response. *Nature* 488, 404–408.

Kuwabara, T., Hsieh, J., Nakashima, K., Taira, K., and Gage, F.H. (2004). A small modulatory dsRNA specifies the fate of adult neural stem cells. *Cell* 116, 779–793.

Langmead, B., and Salzberg, S.L. (2012). Fast gapped-read alignment with Bowtie 2. *Nat. Methods* 9, 357–359.

Larson, J.D., Kasper, L.H., Paugh, B.S., Jin, H., Wu, G., Kwon, C.-H., Fan, Y., Shaw, T.I., Silveira, A.B., Qu, C., et al. (2019). Histone H3.3 K27M Accelerates Spontaneous Brainstem Glioma and Drives Restricted Changes in Bivalent Gene Expression. *Cancer Cell* 35, 140–155.e7.

Laurent, B., Ruitu, L., Murn, J., Hempel, K., Ferrao, R., Xiang, Y., Liu, S., Garcia, B.A., Wu, H., Wu, F., et al. (2015). A specific LSD1/KDM1A isoform regulates neuronal differentiation through H3K9 demethylation. *Mol. Cell* 57, 957–970.

Lee, M.G., Wynder, C., Cooch, N., and Shiekhhattar, R. (2005). An essential role for CoREST in nucleosomal histone 3 lysine 4 demethylation. *Nature* 437, 432–435.

Lewis, P.W., Müller, M.M., Koletsky, M.S., Cordero, F., Lin, S., Banaszynski, L.A., Garcia, B.A., Muir, T.W., Becher, O.J., and Allis, C.D. (2013). Inhibition of PRC2 activity by a gain-of-function H3 mutation found in pediatric glioblastoma. *Science* 340, 857–861.

Li, H., Handsaker, B., Wysoker, A., Fennell, T., Ruan, J., Homer, N., Marth, G., Abecasis, G., Durbin, R., and 1000 Genome Project Data Processing Subgroup (2009). The Sequence Alignment/Map format and SAMtools. *Bioinforma. Oxf. Engl.* 25, 2078–2079.

Liao, Y., Smyth, G.K., and Shi, W. (2014). featureCounts: an efficient general purpose program for assigning sequence reads to genomic features. *Bioinforma. Oxf. Engl.* 30, 923–930.

Liu, T., Ortiz, J.A., Taing, L., Meyer, C.A., Lee, B., Zhang, Y., Shin, H., Wong, S.S., Ma, J., Lei, Y., et al. (2011). Cistrome: an integrative platform for transcriptional regulation studies. *Genome Biol.* 12, R83.

Lu, D., Yan, J., Wang, L., Liu, H., Zeng, L., Zhang, M., Duan, W., Ji, Y., Cao, J., Geng, M., et al. (2017). Design, Synthesis, and Biological Evaluation of the First c-Met/HDAC Inhibitors Based on Pyridazinone Derivatives. *ACS Med. Chem. Lett.* 8, 830–834.

Lunyak, V.V., and Rosenfeld, M.G. (2005). No rest for REST: REST/NRSF regulation of neurogenesis. *Cell* 121, 499–501.

Mack, S.C., Hubert, C.G., Miller, T.E., Taylor, M.D., and Rich, J.N. (2016). An epigenetic gateway to brain tumor cell identity. *Nat. Neurosci.* 19, 10–19.

Matsuda, S., Baba, R., Oki, H., Morimoto, S., Toyofuku, M., Igaki, S., Kamada, Y., Iwasaki, S., Matsumiya, K., Hibino, R., et al. (2019). T-448, a specific inhibitor of LSD1 enzyme activity, improves learning function without causing thrombocytopenia in mice.

*Neuropsychopharmacology* 44, 1505–1512.

Matthay, K.K., Reynolds, C.P., Seeger, R.C., Shimada, H., Adkins, E.S., Haas-Kogan, D., Gerbing, R.B., London, W.B., and Villablanca, J.G. (2009). Long-Term Results for Children With High-Risk Neuroblastoma Treated on a Randomized Trial of Myeloablative Therapy Followed by 13- *cis* -Retinoic Acid: A Children’s Oncology Group Study. *J. Clin. Oncol.* 27, 1007–1013.

McLean, C.Y., Bristor, D., Hiller, M., Clarke, S.L., Schaar, B.T., Lowe, C.B., Wenger, A.M., and Bejerano, G. (2010). GREAT improves functional interpretation of cis-regulatory regions. *Nat. Biotechnol.* 28, 495–501.

Metzger, E., Wissmann, M., Yin, N., Müller, J.M., Schneider, R., Peters, A.H.F.M., Günther, T., Buettner, R., and Schüle, R. (2005). LSD1 demethylates repressive histone marks to promote androgen-receptor-dependent transcription. *Nature* 437, 436–439.

Mohammad, F., Weissmann, S., Leblanc, B., Pandey, D.P., Højfeldt, J.W., Comet, I., Zheng, C., Johansen, J.V., Rapin, N., Porse, B.T., et al. (2017). EZH2 is a potential therapeutic target for H3K27M-mutant pediatric gliomas. *Nat. Med.* 23, 483–492.

Mohammad, H.P., Smitheman, K.N., Kamat, C.D., Soong, D., Federowicz, K.E., Van Aller, G.S., Schneck, J.L., Carson, J.D., Liu, Y., Butticello, M., et al. (2015). A DNA Hypomethylation Signature Predicts Antitumor Activity of LSD1 Inhibitors in SCLC. *Cancer Cell* 28, 57–69.

- Mosammaparast, N., and Shi, Y. (2010). Reversal of Histone Methylation: Biochemical and Molecular Mechanisms of Histone Demethylases. *Annu. Rev. Biochem.* 79, 155–179.
- Nagaraja, S., Vitanza, N.A., Woo, P.J., Taylor, K.R., Liu, F., Zhang, L., Li, M., Meng, W., Ponnuswami, A., Sun, W., et al. (2017). Transcriptional Dependencies in Diffuse Intrinsic Pontine Glioma. *Cancer Cell* 31, 635-652.e6.
- Nechiporuk, T., McGann, J., Mullendorff, K., Hsieh, J., Wurst, W., Floss, T., and Mandel, G. (2016). The REST remodeling complex protects genomic integrity during embryonic neurogenesis. *ELife* 5, e09584.
- Pathania, M., De Jay, N., Maestro, N., Harutyunyan, A.S., Nitarska, J., Pahlavan, P., Henderson, S., Mikael, L.G., Richard-Londt, A., Zhang, Y., et al. (2017). H3.3K27M Cooperates with Trp53 Loss and PDGFRA Gain in Mouse Embryonic Neural Progenitor Cells to Induce Invasive High-Grade Gliomas. *Cancer Cell* 32, 684-700.e9.
- Paugh, B.S., Broniscer, A., Qu, C., Miller, C.P., Zhang, J., Tatevossian, R.G., Olson, J.M., Geyer, J.R., Chi, S.N., da Silva, N.S., et al. (2011). Genome-wide analyses identify recurrent amplifications of receptor tyrosine kinases and cell-cycle regulatory genes in diffuse intrinsic pontine glioma. *J. Clin. Oncol. Off. J. Am. Soc. Clin. Oncol.* 29, 3999–4006.
- Perera, A., Eisen, D., Wagner, M., Laube, S.K., Künzel, A.F., Koch, S., Steinbacher, J., Schulze, E., Splith, V., Mittermeier, N., et al. (2015). TET3 Is Recruited by REST for Context-Specific Hydroxymethylation and Induction of Gene Expression. *Cell Rep.* 11, 283–294.

Pfyster, G.E., Faivre-Bauman, A., Tixier-Vidal, A., Norman, A.W., and Heizmann, C.W. (1987). Developmental and functional studies of parvalbumin and calbindin D28K in hypothalamic neurons grown in serum-free medium. *J. Neurochem.* 49, 442–451.

Piunti, A., Hashizume, R., Morgan, M.A., Bartom, E.T., Horbinski, C.M., Marshall, S.A., Rendleman, E.J., Ma, Q., Takahashi, Y., Woodfin, A.R., et al. (2017). Therapeutic targeting of polycomb and BET bromodomain proteins in diffuse intrinsic pontine gliomas. *Nat. Med.* 23, 493–500.

Prusevich, P., Kalin, J.H., Ming, S.A., Basso, M., Givens, J., Li, X., Hu, J., Taylor, M.S., Cieniewicz, A.M., Hsiao, P.-Y., et al. (2014). A selective phenelzine analogue inhibitor of histone demethylase LSD1. *ACS Chem. Biol.* 9, 1284–1293.

Qian, C., Lai, C.-J., Bao, R., Wang, D.-G., Wang, J., Xu, G.-X., Atoyan, R., Qu, H., Yin, L., Samson, M., et al. (2012). Cancer network disruption by a single molecule inhibitor targeting both histone deacetylase activity and phosphatidylinositol 3-kinase signaling. *Clin. Cancer Res. Off. J. Am. Assoc. Cancer Res.* 18, 4104–4113.

Qin, E.Y., Cooper, D.D., Abbott, K.L., Lennon, J., Nagaraja, S., Mackay, A., Jones, C., Vogel, H., Jackson, P.K., and Monje, M. (2017). Neural Precursor-Derived Pleiotrophin Mediates Subventricular Zone Invasion by Glioma. *Cell* 170, 845-859.e19.

Qureshi, I.A., Gokhan, S., and Mehler, M.F. (2010). REST and CoREST are transcriptional and epigenetic regulators of seminal neural fate decisions. *Cell Cycle* 9, 4477–4486.



- Ramírez, F., Ryan, D.P., Grüning, B., Bhardwaj, V., Kilpert, F., Richter, A.S., Heyne, S., Dündar, F., and Manke, T. (2016). deepTools2: a next generation web server for deep-sequencing data analysis. *Nucleic Acids Res.* 44, W160–W165.
- Robinson, J.T., Thorvaldsdóttir, H., Winckler, W., Guttman, M., Lander, E.S., Getz, G., and Mesirov, J.P. (2011). Integrative genomics viewer. *Nat. Biotechnol.* 29, 24–26.
- Rory Stark<Rory.Stark@Cruk.Cam.Ac.Uk>, G.B.C. (2017). DiffBind.
- Saratsis, A.M., Kambhampati, M., Snyder, K., Yadavilli, S., Devaney, J.M., Harmon, B., Hall, J., Raabe, E.H., An, P., Weingart, M., et al. (2014). Comparative multidimensional molecular analyses of pediatric diffuse intrinsic pontine glioma reveals distinct molecular subtypes. *Acta Neuropathol. (Berl.)* 127, 881–895.
- Schenk, T., Chen, W.C., Göllner, S., Howell, L., Jin, L., Hebestreit, K., Klein, H.-U., Popescu, A.C., Burnett, A., Mills, K., et al. (2012). Inhibition of the LSD1 (KDM1A) demethylase reactivates the all-trans-retinoic acid differentiation pathway in acute myeloid leukemia. *Nat. Med.* 18, 605–611.
- Schoenherr, C.J., and Anderson, D.J. (1995). The neuron-restrictive silencer factor (NRSF): a coordinate repressor of multiple neuron-specific genes. *Science* 267, 1360–1363.
- Schoenherr, C.J., Paquette, A.J., and Anderson, D.J. (1996). Identification of potential target genes for the neuron-restrictive silencer factor. *Proc. Natl. Acad. Sci. U. S. A.* 93, 9881–9886.

Schwartzentruber, J., Korshunov, A., Liu, X.-Y., Jones, D.T.W., Pfaff, E., Jacob, K., Sturm, D., Fontebasso, A.M., Quang, D.-A.K., Tönjes, M., et al. (2012). Driver mutations in histone H3.3 and chromatin remodelling genes in paediatric glioblastoma. *Nature* 482, 226–231.

Shaik, S., Kennis, B., Maegawa, S., Schadler, K., Yanwen, Y., Callegari, K., Lulla, R.R., Goldman, S., Nazarian, J., Rajaram, V., et al. (2018). REST upregulates gremlin to modulate diffuse intrinsic pontine glioma vasculature. *Oncotarget* 9, 5233–5250.

Singh, M.M., Manton, C.A., Bhat, K.P., Tsai, W.-W., Aldape, K., Barton, M.C., and Chandra, J. (2011). Inhibition of LSD1 sensitizes glioblastoma cells to histone deacetylase inhibitors. *Neuro-Oncol.* 13, 894–903.

Stafford, J.M., Lee, C.-H., Voigt, P., Descostes, N., Saldaña-Meyer, R., Yu, J.-R., Leroy, G., Oksuz, O., Chapman, J.R., Suarez, F., et al. (2018). Multiple modes of PRC2 inhibition elicit global chromatin alterations in H3K27M pediatric glioma. *Sci. Adv.* 4, eaau5935.

Strahl, B.D., and Allis, C.D. (2000). The language of covalent histone modifications. *Nature* 403, 41–45.

Sturm, D., Witt, H., Hovestadt, V., Khuong-Quang, D.-A., Jones, D.T.W., Konermann, C., Pfaff, E., Tönjes, M., Sill, M., Bender, S., et al. (2012). Hotspot mutations in H3F3A and IDH1 define distinct epigenetic and biological subgroups of glioblastoma. *Cancer Cell* 22, 425–437.

Subramanian, A., Tamayo, P., Mootha, V.K., Mukherjee, S., Ebert, B.L., Gillette, M.A., Paulovich, A., Pomeroy, S.L., Golub, T.R., Lander, E.S., et al. (2005). Gene set enrichment analysis: a knowledge-based approach for interpreting genome-wide expression profiles. *Proc. Natl. Acad. Sci. U. S. A.* 102, 15545–15550.

Sugino, N., Kawahara, M., Tatsumi, G., Kanai, A., Matsui, H., Yamamoto, R., Nagai, Y., Fujii, S., Shimazu, Y., Hishizawa, M., et al. (2017). A novel LSD1 inhibitor NCD38 ameliorates MDS-related leukemia with complex karyotype by attenuating leukemia programs via activating super-enhancers. *Leukemia* 31, 2303–2314.

Sun, G., Alzayady, K., Stewart, R., Ye, P., Yang, S., Li, W., and Shi, Y. (2010). Histone demethylase LSD1 regulates neural stem cell proliferation. *Mol. Cell. Biol.* 30, 1997–2005.

Usoskin, D., Furlan, A., Islam, S., Abdo, H., Lönnerberg, P., Lou, D., Hjerling-Leffler, J., Haeggström, J., Kharchenko, O., Kharchenko, P.V., et al. (2014). Unbiased classification of sensory neuron types by large-scale single-cell RNA sequencing. *Nat. Neurosci.* 18, 145–153.

Van Dort, M.E., Galbán, S., Wang, H., Sebolt-Leopold, J., Whitehead, C., Hong, H., Rehemtulla, A., and Ross, B.D. (2015). Dual inhibition of allosteric mitogen-activated protein kinase (MEK) and phosphatidylinositol 3-kinase (PI3K) oncogenic targets with a bifunctional inhibitor. *Bioorg. Med. Chem.* 23, 1386–1394.

Vasilatos, S.N., Katz, T.A., Oesterreich, S., Wan, Y., Davidson, N.E., and Huang, Y. (2013). Crosstalk between lysine-specific demethylase 1 (LSD1) and histone deacetylases mediates antineoplastic efficacy of HDAC inhibitors in human breast cancer cells. *Carcinogenesis* 34, 1196–1207.

Venneti, S., Garimella, M.T., Sullivan, L.M., Martinez, D., Huse, J.T., Heguy, A., Santi, M., Thompson, C.B., and Judkins, A.R. (2013). Evaluation of histone 3 lysine 27 trimethylation (H3K27me3) and enhancer of Zest 2 (EZH2) in pediatric glial and glioneuronal tumors shows

decreased H3K27me3 in H3F3A K27M mutant glioblastomas. *Brain Pathol. Zurich Switz.* 23, 558–564.

Westerlund, I., Shi, Y., Toskas, K., Fell, S.M., Li, S., Surova, O., Södersten, E., Kogner, P., Nyman, U., Schlisio, S., et al. (2017). Combined epigenetic and differentiation-based treatment inhibits neuroblastoma tumor growth and links HIF2 $\alpha$  to tumor suppression. *Proc. Natl. Acad. Sci. U. S. A.* 114, E6137–E6146.

Whyte, W.A., Bilodeau, S., Orlando, D.A., Hoke, H.A., Frampton, G.M., Foster, C.T., Cowley, S.M., and Young, R.A. (2012). Enhancer decommissioning by LSD1 during embryonic stem cell differentiation. *Nature* 482, 221–225.

Whyte, W.A., Orlando, D.A., Hnisz, D., Abraham, B.J., Lin, C.Y., Kagey, M.H., Rahl, P.B., Lee, T.I., and Young, R.A. (2013). Master Transcription Factors and Mediator Establish Super-Enhancers at Key Cell Identity Genes. *Cell* 153, 307–319.

Wiese, M., Schill, F., Sturm, D., Pfister, S., Hulleman, E., Johnsen, S.A., and Kramm, C.M. (2016). No Significant Cytotoxic Effect of the EZH2 Inhibitor Tazemetostat (EPZ-6438) on Pediatric Glioma Cells with Wildtype Histone 3 or Mutated Histone 3.3. *Klin. Padiatr.* 228, 113–117.

Wu, G., Broniscer, A., McEachron, T.A., Lu, C., Paugh, B.S., Becksfort, J., Qu, C., Ding, L., Huether, R., Parker, M., et al. (2012). Somatic histone H3 alterations in pediatric diffuse intrinsic pontine gliomas and non-brainstem glioblastomas. *Nat. Genet.* 44, 251–253.

Zambelli, F., Pesole, G., and Pavesi, G. (2013). PscanChIP: Finding over-represented transcription factor-binding site motifs and their correlations in sequences from ChIP-Seq experiments. *Nucleic Acids Res.* *41*, W535-543.

Zee, B.M., Alekseyenko, A.A., McElroy, K.A., and Kuroda, M.I. (2016). Streamlined discovery of cross-linked chromatin complexes and associated histone modifications by mass spectrometry. *Proc. Natl. Acad. Sci. U. S. A.* *113*, 1784–1789.

Zhang, Y., Liu, T., Meyer, C.A., Eeckhoutte, J., Johnson, D.S., Bernstein, B.E., Nusbaum, C., Myers, R.M., Brown, M., Li, W., et al. (2008). Model-based analysis of ChIP-Seq (MACS). *Genome Biol.* *9*, R137.

## KEY RESOURCES TABLE

| REAGENT or RESOURCE                                  | SOURCE                             | IDENTIFIER         |
|--|------------------------------------|--------------------|
| <b>Antibodies</b>                                    |                                    |                    |
| Mouse $\alpha$ -Human Nucleoli antibody              | Abcam                              | ab190710 1         |
| Rabbit $\alpha$ -H3K4me2                             | Millipore                          | 07-030             |
| Rabbit $\alpha$ -H3K27me3                            | Millipore                          | 07-449             |
| Rabbit $\alpha$ -H4 pan-acetyl                       | Abcam                              | ab10807            |
| Rabbit $\alpha$ -H3K27ac                             | Active Motif                       | 39135              |
| Rabbit $\alpha$ -H3K4me1                             | Abcam                              | ab8895             |
| Rabbit $\alpha$ -Histone H3                          | Abcam                              | ab1791             |
| Mouse $\alpha$ -CALB1                                | In house                           | Dr. Stefanie Giera |
| Mouse $\alpha$ -NP2 (G-9)                            | Santa Cruz Biotechnology           | sc-166035          |
| Mouse $\alpha$ -Ki67                                 | DAKO                               | M7240              |
| Mouse $\alpha$ -BrdU (Bu20a)                         | Cell Signaling Technology          | 5292S              |
| Mouse $\alpha$ -SYNI/II/II                           | Biolegend                          | #801202            |
| c-Caspase 3  | ServiceBio                         | GB11009            |
| Ki67 (IHC)   | ServiceBio                         | GB13030-2          |
| Rabbit $\alpha$ -KDM1 (LSD1)                         | Abcam                              | ab17721            |
| Rabbit $\alpha$ -H3K27M                              | EMD Millipore                      | ABE419             |
| Anti- $\beta$ -Tubulin, clone AA2                    | EMD Millipore                      | 05-661             |
| <b>Bacterial and Virus Strains</b>                   |                                    |                    |
| One Shot® Stbl3™ Chemically Competent E. coli        | Life Technologies (Invitrogen)     | C737303            |
|  |                                    |                    |
| <b>Biological Samples</b>                            |                                    |                    |
|  |                                    |                    |
|  |                                    |                    |
|  |                                    |                    |
|  |                                    |                    |
|  |                                    |                    |
| <b>Chemicals, Peptides, and Recombinant Proteins</b> |                                    |                    |
| Corin  | Dr. Phil Cole                      | n/a                |
| Compound 7   | Dr. Phil Cole                      | n/a                |
| MS275  | Dr. Phil Cole                      | n/a                |
| JQ1  | The Structural Genomics Consortium | n/a                |
| Bromosporin (BSP)                                    | The Structural Genomics Consortium | n/a                |
| IBET-151   | The Structural Genomics Consortium | n/a                |
| PFI-1  | The Structural Genomics Consortium | n/a                |
| UNC0642  | The Structural Genomics Consortium | n/a                |
| UNC0638  | The Structural Genomics Consortium | n/a                |
| PFI-3  | The Structural Genomics Consortium | n/a                |

|   |                                    |              |
|---|------------------------------------|--------------|
| IOX2                                      | The Structural Genomics Consortium | n/a          |
| GSK-2801                                  | The Structural Genomics Consortium | n/a          |
| ICBP-112                                  | The Structural Genomics Consortium | n/a          |
| CI-994                                    | The Structural Genomics Consortium | n/a          |
| LAQ824                                    | The Structural Genomics Consortium | n/a          |
| Panobinostat (LBH589)                     | Selleck Chemicals                  | S1030        |
| GSK-LSD1                                  | The Structural Genomics Consortium | n/a          |
| IOX1                                      | The Structural Genomics Consortium | n/a          |
| LLY507                                    | The Structural Genomics Consortium | n/a          |
| OICR9429                                  | The Structural Genomics Consortium | n/a          |
| UNC1999                                   | The Structural Genomics Consortium | n/a          |
| SGC-0946                                  | The Structural Genomics Consortium | n/a          |
| PFI-2                                     | The Structural Genomics Consortium | n/a          |
| UNC1215                                   | The Structural Genomics Consortium | n/a          |
| Human EGF                                 | Shenandoah Biotechnology Inc.      | 100-26-500µg |
| Human PDGF-BB                             | Shenandoah Biotechnology Inc.      | 100-18-100µg |
| Human PDGF-AA                             | Shenandoah Biotechnology Inc.      | 100-16-100µg |
| Recombinant Human FGF-basic (154 a.a.)    | Shenandoah Biotechnology Inc.      | 100-18B      |
| 0.2% Heparin Sodium Salt in PBS           | STEMCELL Technologies              | 07980        |
| Neurobasal®-A Medium                      | Thermo Fisher Scientific           | 10888022     |
| DMEM/F-12, HEPES                          | Thermo Fisher Scientific           | 11330057     |
| DMEM                                      | Thermo Fisher Scientific           | 11995073     |
| GlutaMAX™ Supplement                      | Thermo Fisher Scientific           | 35050-061    |
| Antibiotic-Antimycotic Solution (100X)    | Caisson Labs                       | ABL02-100ml  |
| Penicillin-Streptomycin Solution (100x)   | Thermo Fisher Scientific           | 15140122     |
| Fetal Bovine Serum                        | Gemini Bioproducts                 | 900-108      |
| Sodium Pyruvate Solution                  | Caisson Laboratories               | PYL01-100ML  |
| Non-Essential Amino Acids Solution (100x) | Caisson Laboratories               | NAL03-100ML  |
| Polybrene                                 | Millipore Sigma                    | TR-1003-G    |

|   |   |                        |
|---|---|------------------------|
| HEPES Solution 1M solution (228.3 g/L HEPES) in purified water.           | Caisson Laboratories  | HOL06-100ML            |
| Polyethylenimine 25,000 MW  | Polysciences Inc.   | 239-68-3               |
| Polyethylene glycol (PEG) 8000 MW   | Amresco   | 25322-68-3             |
| 16% Paraformaldehyde (formaldehyde) aqueous solution                      | Electron Microscopy Sciences  | 15710                  |
| Blasticidin S Hydrochloride   | Research Products International   | B12200-0.025           |
| Puromycin Dihydrochloride   | Gold Biotechnology  | P-600-500              |
| Trypan Blue Solution, 0.4%  | Thermo Fisher Scientific  | 15250061               |
| TrypLE™ Express Enzyme (1X), no phenol red                                | Thermo Fisher Scientific  | 12604013               |
| RNase A, DNase and protease-free (10 mg/mL)                               | Thermo Fisher Scientific  | EN0531                 |
| Micrococcal Nuclease  | New England Biotechnology   | M0247S                 |
| Proteinase K  | Sigma   | G1508                  |
| RNase   | Roche   | 11119915001            |
| DNA ligase  | New England Biolabs   | M2200S                 |
| PFU ULTRA II Hotstart 2X PCR master mix                                   | Agilent   | 600850                 |
| PureProteome Protein G Magnetic Beads                                     | EMD Millipore   | LSKMAGG02              |
| TRIzol Reagent  | Thermo Fisher Scientific  | 15596018               |
| D-luciferin potassium salt  | Promega   | E1605                  |
| G-418 sodium salt   | Research Products International   | 108321-42-2            |
| Glycogen  | Roche   | 10901393001            |
| Propidium Iodide  | Sigma   | P4170                  |
| <b>Critical Commercial Assays</b>   |   |                        |
| CellTiter-Glo Luminescent Cell Viability Assay                            | Promega   | G7572                  |
| DeadEnd™ Fluorometric TUNEL System  | Promega   | G3250                  |
| NEBNext® Ultra™ DNA Library Prep Kit for Illumina®                        | New England Biolabs   | E7370L                 |
| NEBNext® Multiplex Oligos for Illumina® (Index Primers Set 1)             | New England Biolabs   | E7335L                 |
| NEBNext Poly(A) mRNA isolation module                                     | New England Biolabs   | E7490L                 |
| Virtual Kit: LightCycler® 480 SYBR Green I Master                         | Roche   | 06649416001            |
| PrimeScript™ Reverse Transcriptase Kit                                    | Clontech  | RR037B                 |
| Platinum® PCR SuperMix  | Thermo Fisher Scientific  | 11306016               |
| QIAquick Gel Extraction Kit   | Qiagen  | 28706                  |
| End-It DNA End-Repair Kit   | Epicenter   | ER0720                 |
| <b>Deposited Data</b>   |   |                        |
| Unprocessed mass spectrometry files (.RAW format)                         | <a href="https://dataverse.harvard.edu/link">https://dataverse.harvard.edu/link</a> | doi:10.7910/DVN/HCIXPN |
| chIP-seq with H3K4me1, H3K27ac, H3K27me3, and H3K27M in SU-DIPGXIII cells |   | GEO series GSE110572   |



|   |   |                                 |
|---|---|---------------------------------|
| REST ChIPseq in U87 cells   | <a href="https://www.ncbi.nlm.nih.gov/geo/query/acc.cgi?acc=GSM803372">https://www.ncbi.nlm.nih.gov/geo/query/acc.cgi?acc=GSM803372</a> | GEO series GSM803372            |
| RNA-seq in SU-DIPGXIII cells treated with DMSO, compound 7, MS-275, or Corin.   | <a href="#">link</a>  | GEO series GSE110572            |
| Somatic Histone H3 Mutations in Diffuse Intrinsic Pontine Gliomas and Non-Brainstem Paediatric Glioblastomas  | <a href="https://www.ebi.ac.uk/ega/datasets/EGAD00001000793">https://www.ebi.ac.uk/ega/datasets/EGAD00001000793</a>                     | <a href="#">EGAD00001000793</a> |
| Genome-wide Analyses of Diffuse Intrinsic Pontine Gliomas (Paugh et al. 2011)   | <a href="https://www.ncbi.nlm.nih.gov/geo/query/acc.cgi?acc=GSE26576">https://www.ncbi.nlm.nih.gov/geo/query/acc.cgi?acc=GSE26576</a>   | GEO series GSE26576             |
| H3.3K27M cooperates with p53 loss and Pdgfra gain in mouse embryonic neural progenitor cells to induce invasive high-grade gliomas [Human RNA-Seq] (Pathania et al. 2017) | <a href="https://www.ncbi.nlm.nih.gov/geo/query/acc.cgi?acc=GSE95277">https://www.ncbi.nlm.nih.gov/geo/query/acc.cgi?acc=GSE95277</a>   | GEO series GSE95277             |
| <b>Experimental Models: Cell Lines</b>  |   |                                 |
| SU-DIPGXIII   | Dr. Michelle Monje  | n/a                             |
| SU-DIPGVI   | Dr. Michelle Monje  | n/a                             |
| SU-DIPGIV   | Dr. Michelle Monje  | n/a                             |
| BT869   | Dr. Keith Ligon   | n/a                             |
| BT245   | Dr. Keith Ligon   | n/a                             |
| NHA-hTERT   | Dr. Nada Jabado   | n/a                             |
| HSJD-DIPG007  | Dr.'s Jaume Mora and Angel Montero Carcaboso  | n/a                             |
| HEK293T   | ATCC  | <a href="#">CRL-3216™</a>       |
| BJ normal human fibroblasts   | ATCC  | <a href="#">CRL-2522™</a>       |
| mNSCs -/- tp53  | Dr. Hongwu Zheng  | n/a                             |
| <b>Experimental Models: Organisms/Strains</b>   |   |                                 |
| NOD.Cg-Prkdc <sup>scid</sup> Il2rg <sup>tm1Wjl</sup> /SzJ   | The Jackson Laboratory  | Strain# 005557                  |
| <b>Oligonucleotides</b>   |   |                                 |
| Please see Table S5.  |   |                                 |
| <b>Recombinant DNA</b>  |   |                                 |
| pCMV-dR8.2 dvpr   | Addgene   | Plasmid #8455                   |
| pCMV-VSV-G  | Addgene   | Plasmid #8454                   |
| lentiCas9-Blast   | Addgene   | Plasmid #52962                  |
| pXPR_011  | David Root  | Addgene plasmid# 59702          |
| pLenti SpBsmBI sgRNA Hygro  | Addgene   | Plasmid #62205                  |
| pHIV-Luc-ZsGreen  | Addgene   | Plasmid #39196                  |
| pCDH-flag-H3.3_wt   | Dr. Laura Banaszynski   |                                 |
| pCDH-flag-H3.3_K27M   | Dr. Laura Banaszynski   |                                 |

| Software and Algorithms          |   |   |
|----------------------------------|---|---|
| R                                | R Development Core Team, 2010                 | <a href="https://www.r-project.org/">https://www.r-project.org/</a>   |
| STARS                            | Broad Institute Genetic Perturbation Platform | <a href="https://portals.broadinstitute.org/gpp/public/software/stars">https://portals.broadinstitute.org/gpp/public/software/stars</a>         |
| GraphPad Prism version 7         |   | <a href="https://www.graphpad.com/scientific-software/prism/">https://www.graphpad.com/scientific-software/prism/</a>                           |
| Cytoscape                        | Shannon et. al 2003                           | <a href="http://www.cytoscape.org/">http://www.cytoscape.org/</a>   |
| Bowtie2                          | Langmead and Salzberg, 2012                   | <a href="http://bowtie-bio.sourceforge.net/bowtie2/index.shtml">http://bowtie-bio.sourceforge.net/bowtie2/index.shtml</a>                       |
| Trimmomatic                      | Bolger et al., 2014                           | <a href="http://www.usadellab.org/cms/?page=trimmomatic">http://www.usadellab.org/cms/?page=trimmomatic</a>                                     |
| Trim Galore!                     |   | <a href="https://www.bioinformatics.babraham.ac.uk/projects/trim_galore/">https://www.bioinformatics.babraham.ac.uk/projects/trim_galore/</a>   |
| Subread package                  | Liao et al., 2014                             | <a href="http://subread.sourceforge.net/">http://subread.sourceforge.net/</a>   |
| DeSEQ2                           | Love et. al 2014                              | <a href="https://bioconductor.org/packages/release/bioc/html/DESeq2.html">https://bioconductor.org/packages/release/bioc/html/DESeq2.html</a>   |
| pheatmap                         | Kolde, 2014                                   | <a href="https://cran.r-project.org/web/packages/pheatmap/index.html">https://cran.r-project.org/web/packages/pheatmap/index.html</a>           |
| CEAS                             | Ji et al., 2006                               | <a href="http://liulab.dfci.harvard.edu/CEAS/">http://liulab.dfci.harvard.edu/CEAS/</a>   |
| Cistrome                         | Liu et al., 2011                              | <a href="http://cistrome.org/ap/root">http://cistrome.org/ap/root</a>   |
| GlioVis                          | Bowman et al., 2016                           | <a href="http://gliovis.bioinfo.cnio.es/">http://gliovis.bioinfo.cnio.es/</a>   |
| deepTools                        | Ramirez et al., 2016                          | <a href="https://deeptools.readthedocs.io/en/latest/">https://deeptools.readthedocs.io/en/latest/</a>   |
| DiffBind                         | Stark, 2012                                   | <a href="http://bioconductor.org/packages/release/bioc/html/DiffBind.html">http://bioconductor.org/packages/release/bioc/html/DiffBind.html</a> |
| Picard Tools                     | Broad Institute                               | <a href="http://broadinstitute.github.io/picard/">http://broadinstitute.github.io/picard/</a>   |
| Integrated Genomics Viewer (IGV) | Robinson et al., 2011                         | <a href="http://software.broadinstitute.org/software/igv/">http://software.broadinstitute.org/software/igv/</a>                                 |
| Gene Ontology Analysis           | The Gene Ontology Consortium, 2017            | <a href="http://www.geneontology.org/">http://www.geneontology.org/</a>   |
| UCSC Table Browser               | Karolchik et al., 2004                        | <a href="https://genome.ucsc.edu/cgi-bin/hgTables">https://genome.ucsc.edu/cgi-bin/hgTables</a>   |

|  |                       |   |
|--|-----------------------|---|
| FlowJo   |                       | <a href="https://www.flowjo.com/">https://www.flowjo.com/</a>   |
| MACS2  | Zhang et al., 2008    | <a href="https://github.com/taoliu/MACS">https://github.com/taoliu/MACS</a>   |
| Genomic Regions Enrichment of Annotations Tool (GREAT) | McLean et al., 2010   | <a href="http://great.stanford.edu/public/html/">http://great.stanford.edu/public/html/</a>                           |
| STAR   | Dobin et al., 2013    | <a href="https://github.com/alexdobin/STAR">https://github.com/alexdobin/STAR</a>                                     |
| PSCANChIP  | Zambelli et al. 2013  | <a href="http://www.beaconlab.it/pscan_chip_dev/">http://www.beaconlab.it/pscan_chip_dev/</a>                         |
| MEME suite and FIMO                                    | Grant et al. 2011     | <a href="http://meme-suite.org/tools/fimo">http://meme-suite.org/tools/fimo</a>                                       |
| CellProfiler   | Carpenter et al. 2006 | <a href="https://cellprofiler.org/">https://cellprofiler.org/</a>   |
| SAMtools   | Li et al. 2009        | <a href="http://samtools.sourceforge.net/">http://samtools.sourceforge.net/</a>                                       |
| ROSE (Rank Ordering of Super Enhancers)                | Whyte et al. 2013     | <a href="http://younglab.wi.mit.edu/super_enhancer_code.html">http://younglab.wi.mit.edu/super_enhancer_code.html</a> |

Figure 1

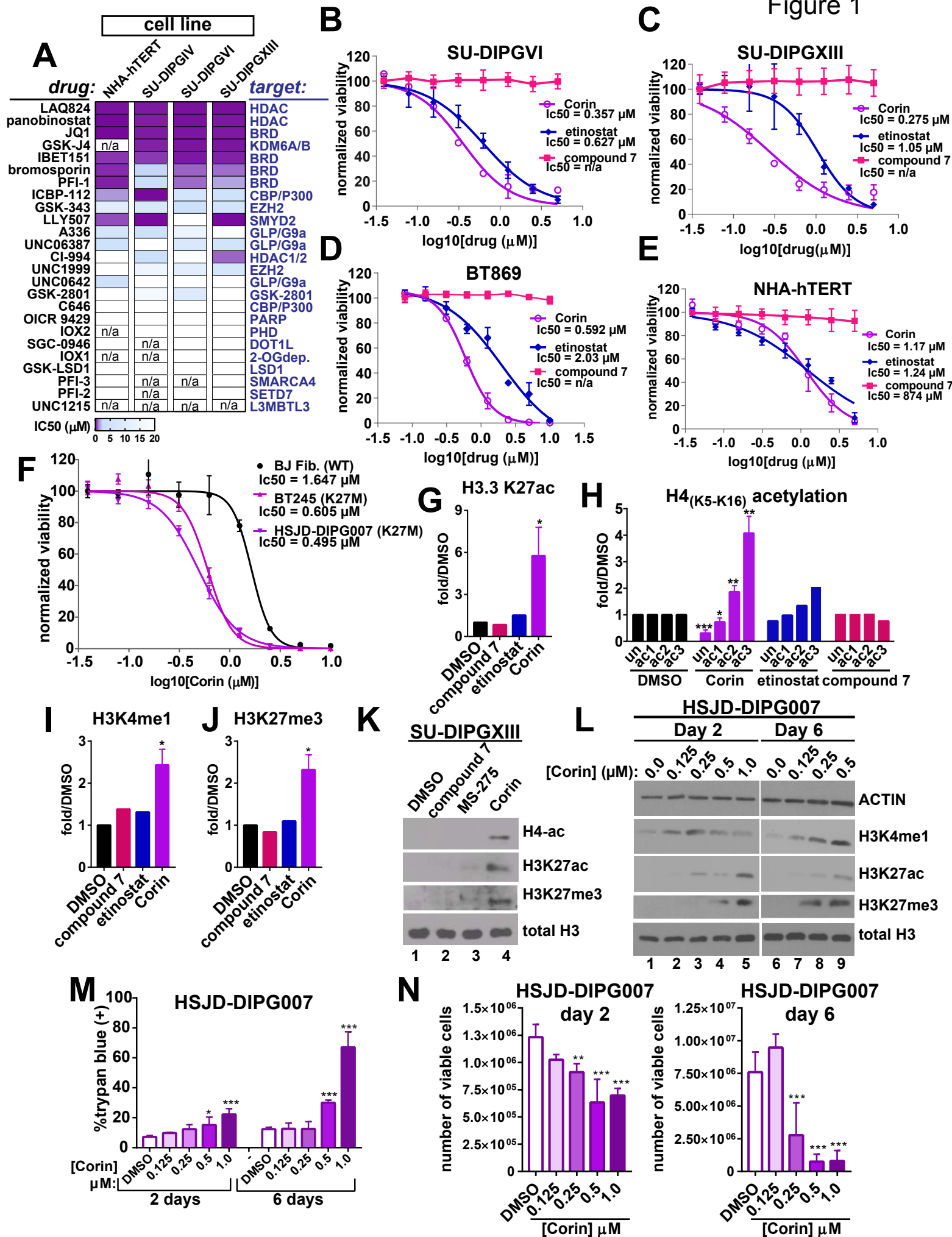


Figure 2

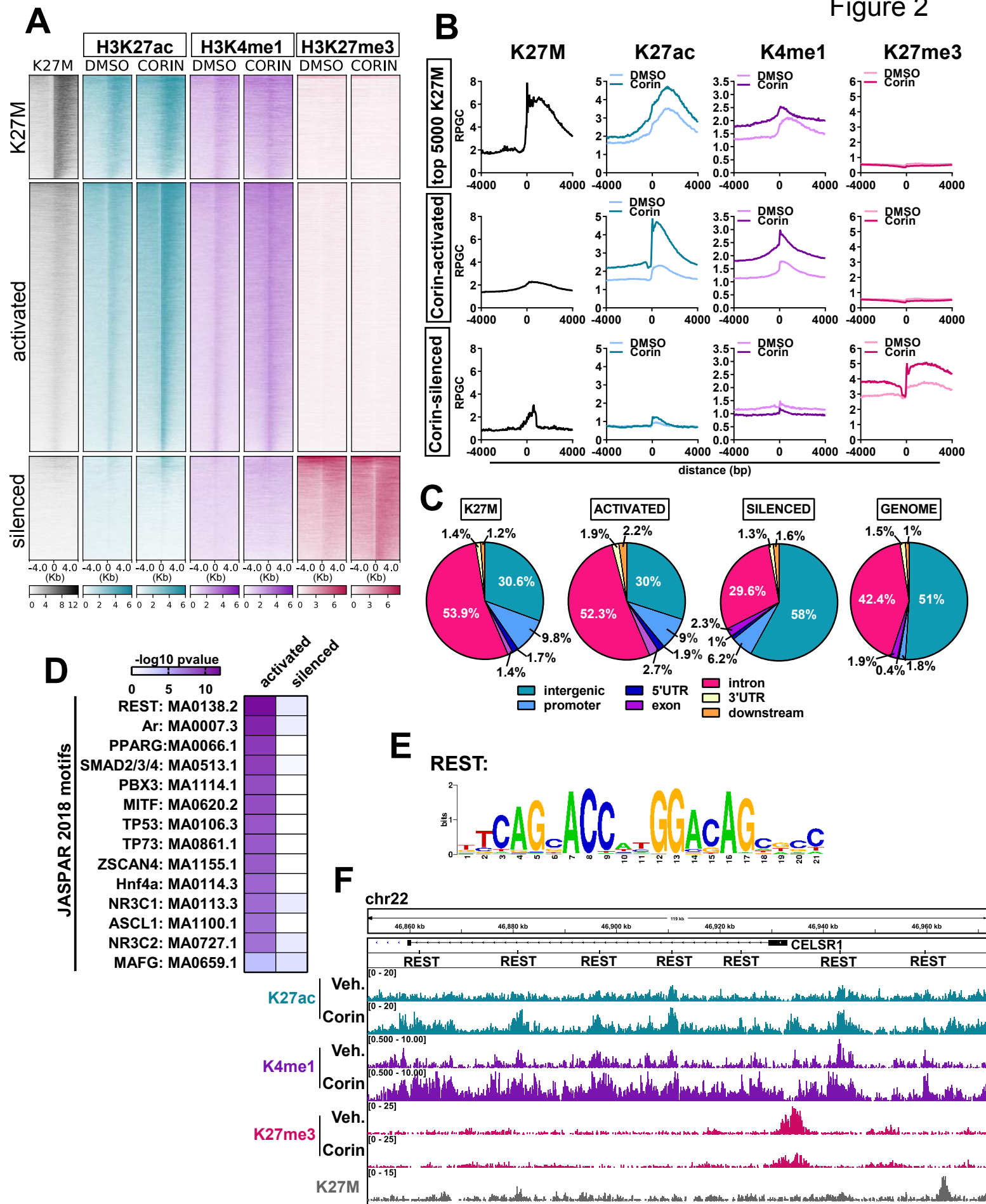


Figure 3

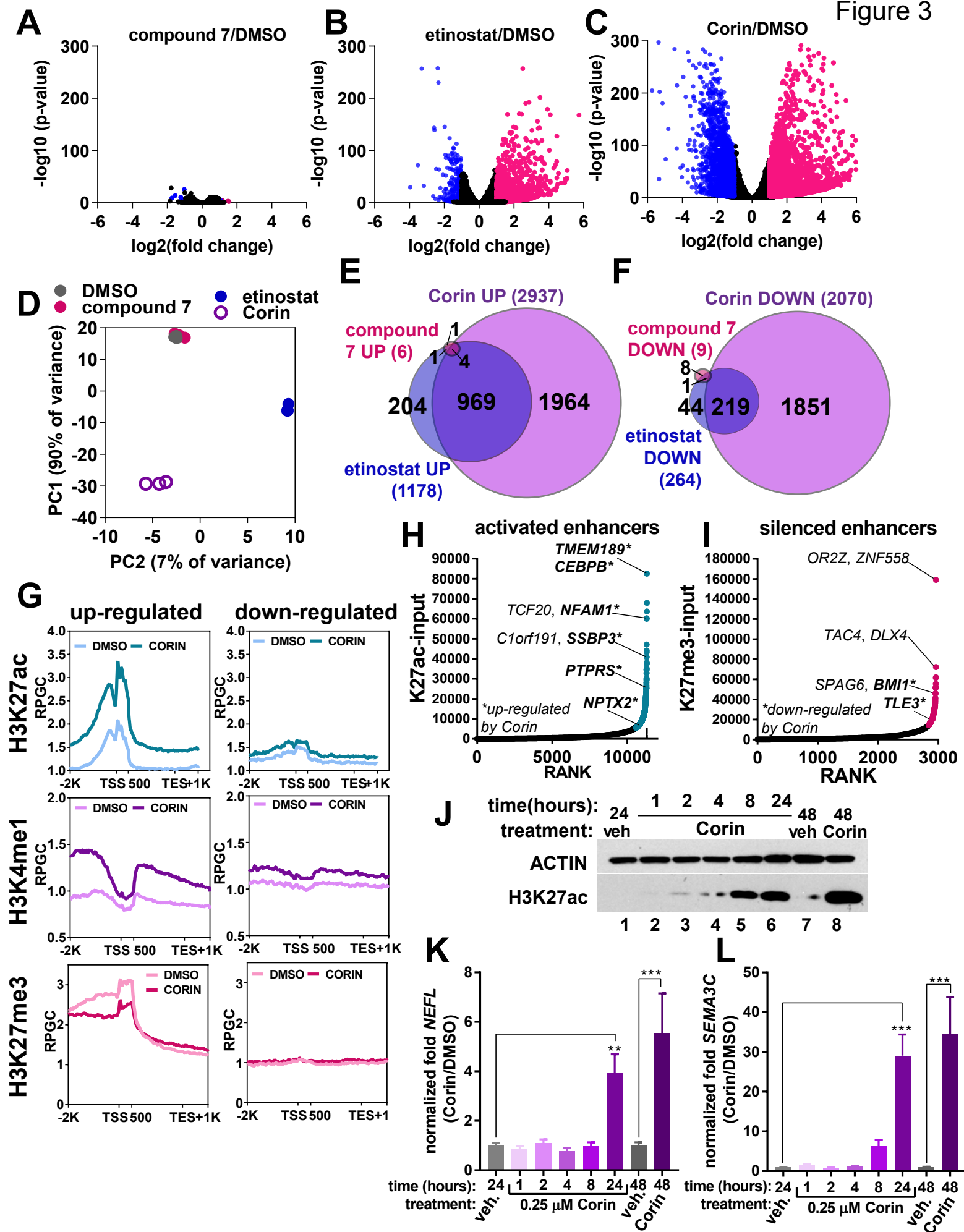




Figure 4

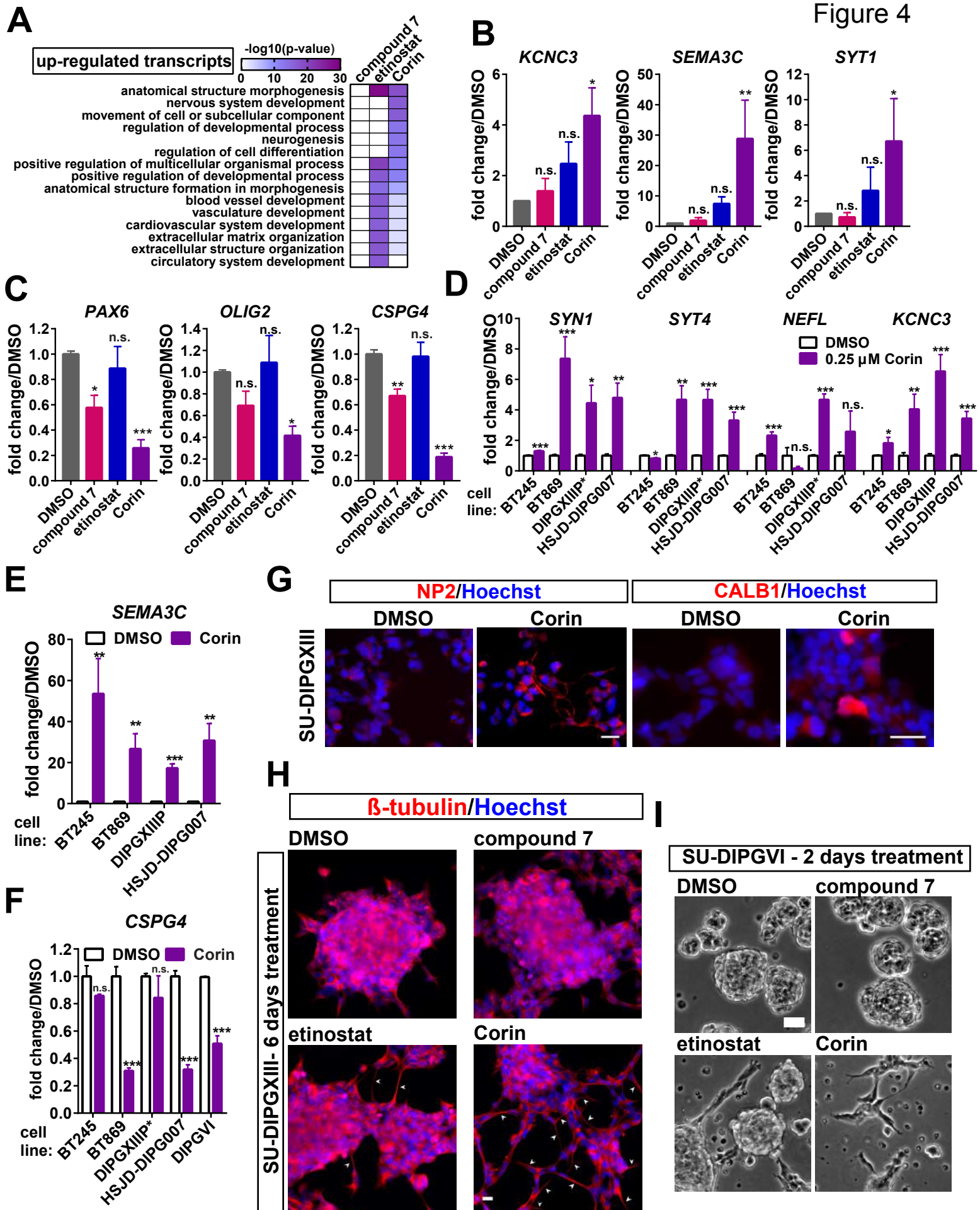


Figure 5

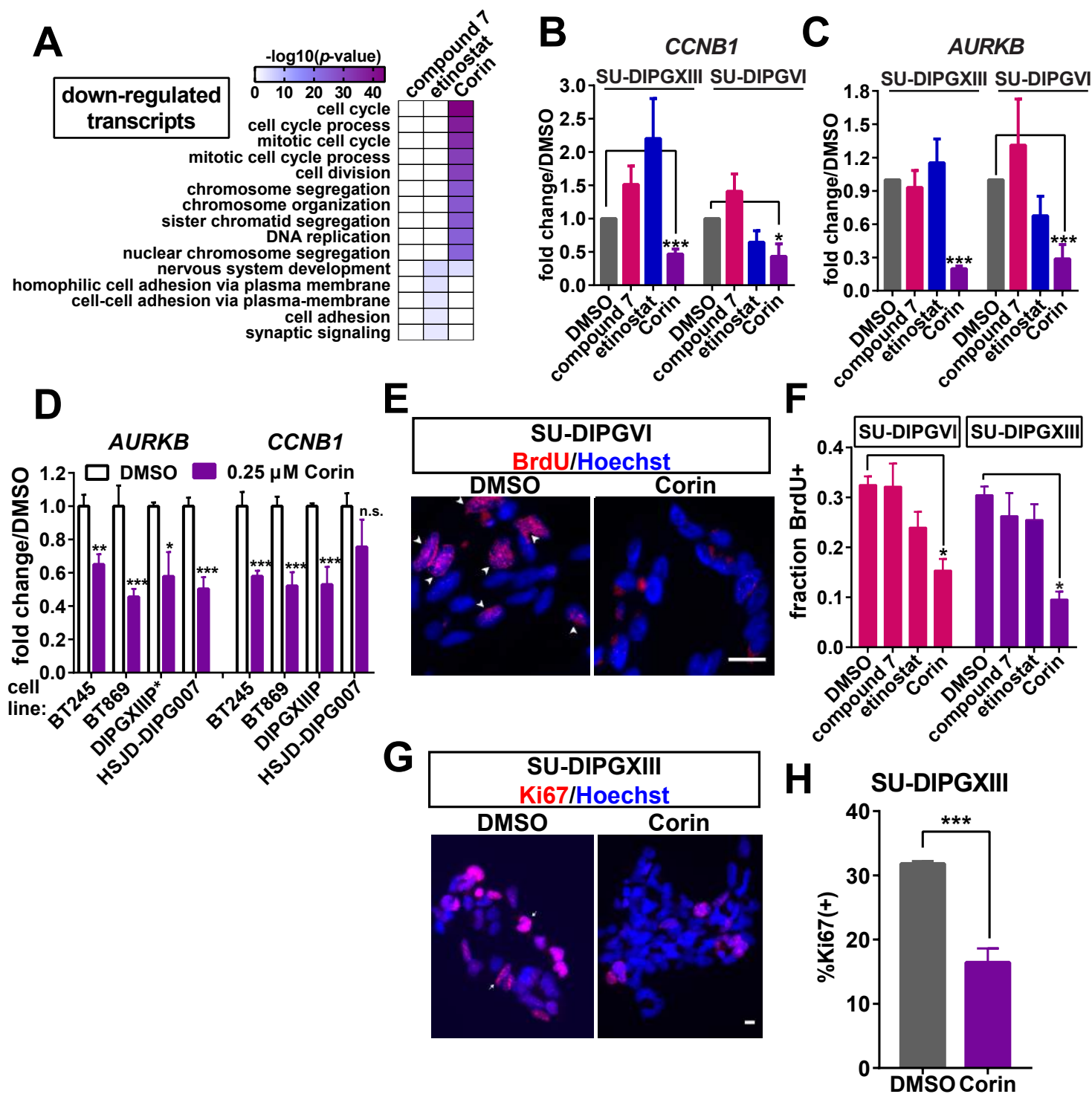




Figure 6

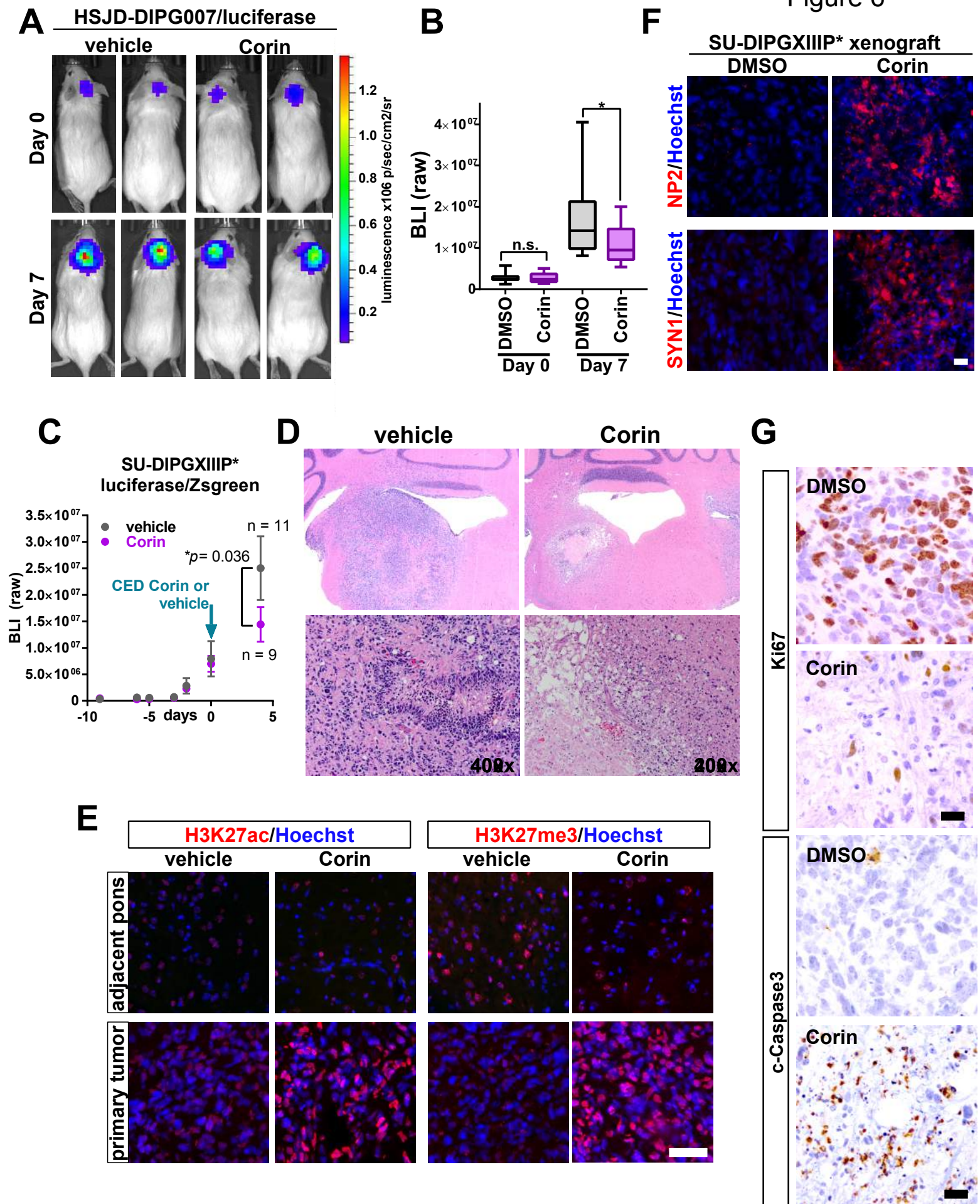
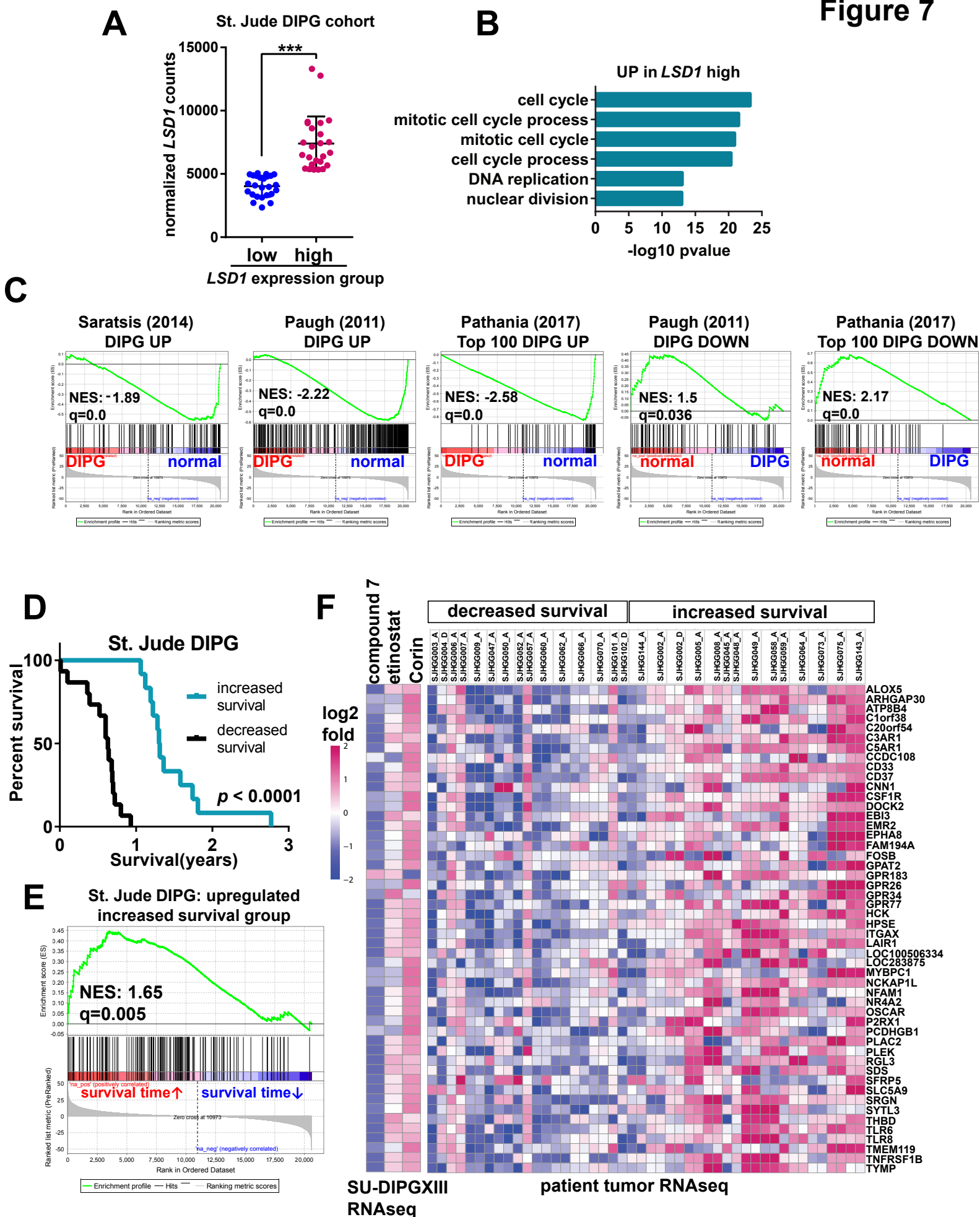


Figure 7



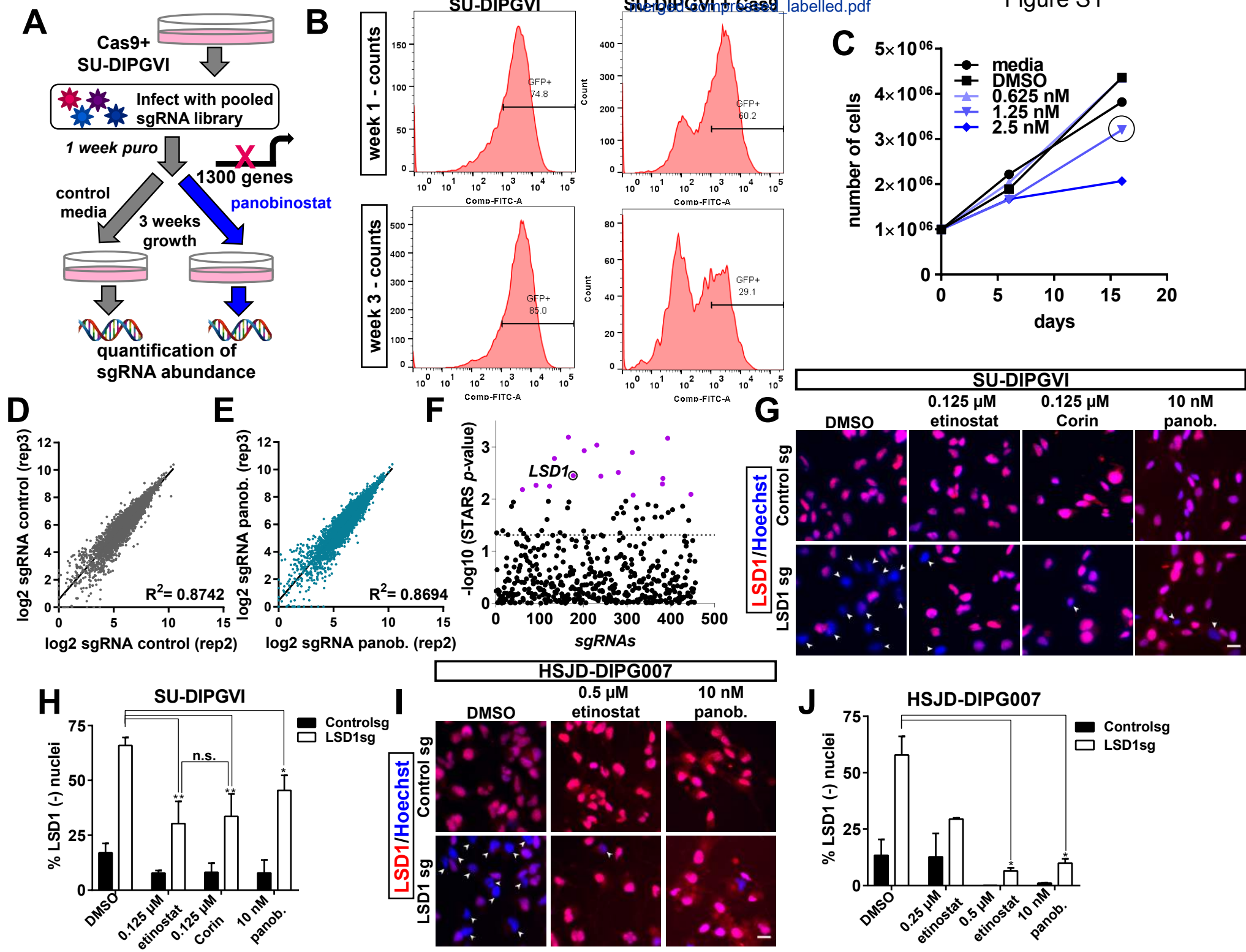




Figure S2

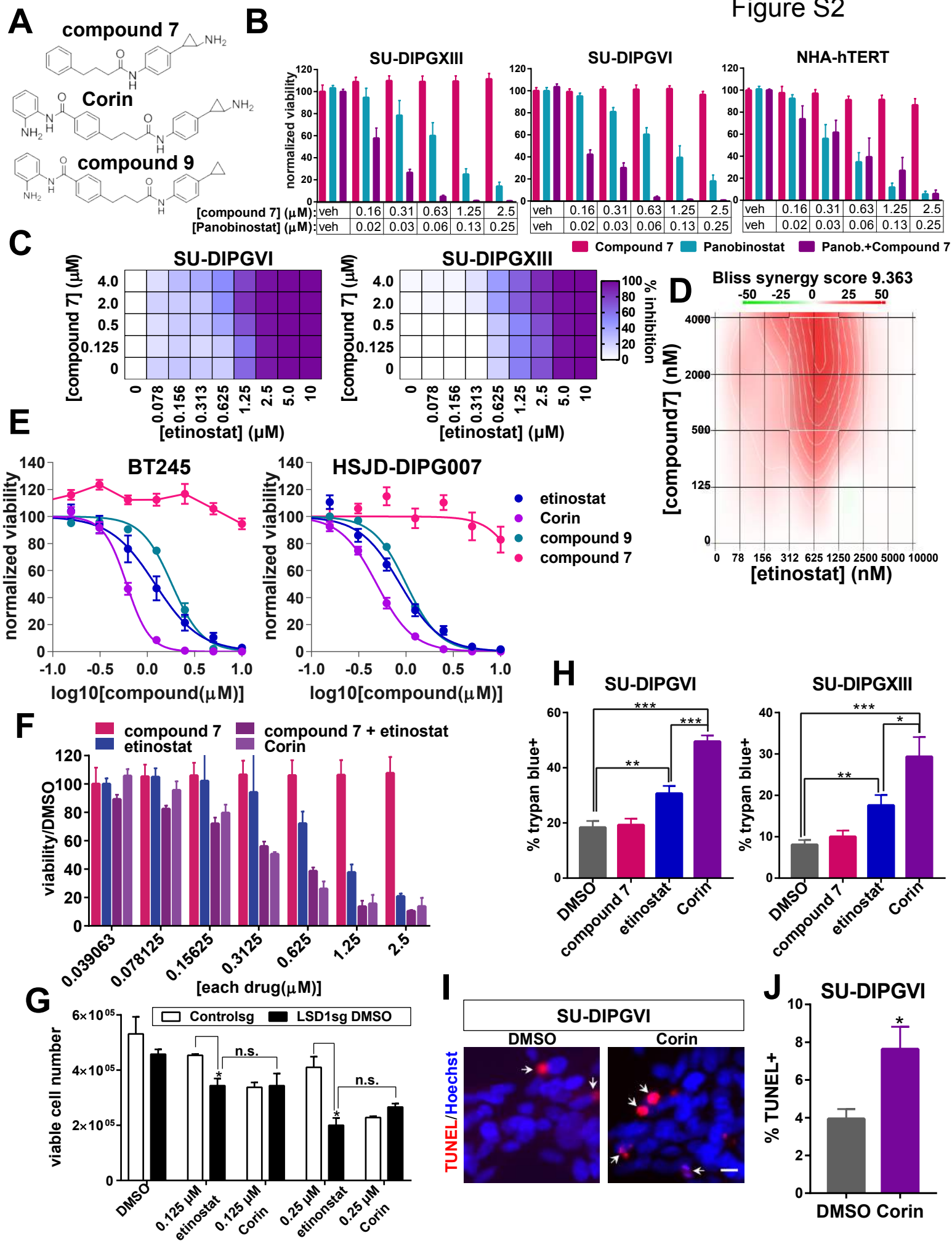




Figure S4

